Development of carbon monoxide-releasing molecules conjugated to polysaccharides (glyco-CORMs) for delivering CO during obesity

Shruti Mohan, Louis-Antoine Barel, Djamal Eddine Benrahla, Bernard Do, Qiyue Mao, Hiroaki Kitagishi, Michael Rivard, Roberto Motterlini, Roberta Foresti

Pharmacological Research 191 (2023) 106770

Contents lists available at ScienceDirect

Pharmacological Research

journal homepage: www.elsevier.com/locate/yphrs

Development of carbon monoxide-releasing molecules conjugated to polysaccharides (glyco-CORMs) for delivering CO during obesity

Shruti Mohan [a,1], Louis-Antoine Barel [b,1], Djamal Eddine Benrahla [a], Bernard Do [c,d], Qiyue Mao [e], Hiroaki Kitagishi [e], Michael Rivard [b], Roberto Motterlini [a,*,2,3], Roberta Foresti [a,*,2,4]

[a] University Paris-Est Créteil, INSERM, IMRB, F-94010, Créteil, France
[b] ICMPE (UMR 7182), CNRS, UPEC, University Paris Est, F-94320 Thiais, France
[c] Materials and Health, University Paris-Saclay, 91400 Orsay, France
[d] Department of Pharmacy, Henri Mondor Hospital, AP-HP, 94000 Créteil, France
[e] Department of Molecular Chemistry and Biochemistry, Faculty of Science and Engineering, Doshisha University, Kyotanabe, Kyoto 610-0321, Japan

ARTICLE INFO

Keywords:
Carbon monoxide
Carbon monoxide-releasing molecules (CO-RMs)
Obesity
Adipocytes
Macrophages

ABSTRACT

Metal carbonyls have been developed as carbon monoxide-releasing molecules (CO-RMs) to deliver CO for therapeutic purposes. The manganese-based CORM-401 has been recently reported to exert beneficial effects in obese animals by reducing body weight gain, improving glucose metabolism and reprogramming adipose tissue towards a healthy phenotype. Here, we report on the synthesis and characterization of glyco-CORMs, obtained by grafting manganese carbonyls on dextrans (70 and 40 kDa), based on the fact that polysaccharides facilitate the targeting of drugs to adipose tissue. We found that glyco-CORMs efficiently deliver CO to cells *in vitro* with higher CO accumulation in adipocytes compared to other cell types. Oral administration of two selected glyco-CORMs (**5b** and **6b**) resulted in CO accumulation in various organs, including adipose tissue. In addition, glyco-CORM **6b** administered for eight weeks elicited anti-obesity and positive metabolic effects in mice fed a high fat diet. Our study highlights the feasibility of creating carriers with multiple functionalized CO-RMs.

1. Introduction

Heme oxygenase-1 (HO-1), an inducible stress-responsive enzymatic protein, degrades heme to carbon monoxide (CO) and biliverdin in all mammalian tissues [1,2]. Induction of HO-1 has been reported to be associated with antioxidant and anti-inflammatory effects [3,4] and several studies have corroborated the crucial role of the HO-1 pathway in alleviating organ and tissue dysfunction in a variety of disease models. These include, among others, ischemia-reperfusion injury [5], organ rejection [6], vascular inflammation [7–9], infection [10] and metabolic disorders such as obesity and diabetes [11–13]. The protective actions of HO-1 can be recapitulated by carbon monoxide (CO) since delivery of controlled amounts of this gas has been reported to exert therapeutic benefits in vascular, ischemic and metabolic disorders [2,14–16]. Our group has pioneered the discovery of CO-releasing molecules (CO-RMs) to deliver controlled amounts of CO to biological systems and confirmed their therapeutic applicability in vascular, ischemic and inflammatory diseases [17–21]. We previously reported that oral

Abbreviations: ATP, Adenosine triphosphate; CDI, carbonyldiimidazole; CO, carbon monoxide; CO-RMs, CO-releasing molecules; COHb, carboxyhemoglobin; D70 Dextran, 70 kDa; D40 Dextran, 40 kDa; DCM, dichloromethane; DMEM, Dulbecco's Modified Eagle's Medium; DMF, dimethylformamide; DMSO, dimethyl sulfoxide; DPBS, Dulbecco's Phosphate Buffer Solution; ECAR, extracellular acidification rate; EDC, 1-Ethyl-3-(3-dimethylaminopropyl)carbodiimide; FBS, Fetal Bovine Serum; FCCP, carbonyl cyanide 4-(trifluoromethoxy) phenylhydrazone; GTT, glucose tolerance tests; HFD, high fat diet; IBMX, 3-isobutyl-1-methylxanthine; ITT, insulin tolerance tests; OCR, oxygen consumption rate; LPS, Lipopolysaccharide.

* Correspondence to: INSERM U955, Faculty of Health, University Paris-Est, 8 Rue du Général Sarrail, 94010 Creteil, France.
E-mail addresses: roberto.motterlini@inserm.fr (R. Motterlini), roberta.foresti@inserm.fr (R. Foresti).
[1] These authors equally contributed to the article.
[2] These authors are co-senior and co-corresponding authors.
[3] https://orcid.org/0000-0003-2684-2612
[4] https://orcid.org/0000-0002-0836-7937

https://doi.org/10.1016/j.phrs.2023.106770
Received 10 March 2023; Received in revised form 6 April 2023; Accepted 13 April 2023
Available online 15 April 2023

administration of a water-soluble manganese-based CO carrier (CORM-401, hereafter **401**) [22] promotes weight loss and counteracts the impairment of metabolism in obese mice *via* a mechanism that involves uncoupling of mitochondrial respiration in adipose tissue [23]. Mitochondrial uncoupling is a process that promotes entrance of protons from the mitochondrial inter-membrane space into the matrix, driving electron transport and O_2 consumption in the respiratory chain in a manner that is completely independent from ATP synthesis. The result is a short-circuit that dissipates energy as heat, a phenomenon well described in brown adipose tissue [24]. In line with this, we have recently shown that **401** increases body temperature in rats in the early hours following oral administration [25].

Uncoupling is also investigated as a strategy to increase energy expenditure and reduce adiposity for beneficial metabolic outcomes in obesity and diabetes [26]. Still in relation to metabolism, previous studies reported that CORM-A1, another pharmacologically active CO releaser, reduces body weight and improves glucose tolerance and insulin sensitivity while decreasing hepatic steatosis [27,28]. Interestingly, CORM-A1-treated mice exhibited a significant increase in oxygen consumption that was twice as high as the levels of oxygen consumption observed in control obese mice [27,28], suggesting a strong link between mitochondrial bioenergetics and weight loss.

Assessing the distribution of CO in the organism following activation of HO-1 by hemin or administration of CO gas or CO-RMs is an important step to understand the mechanisms of action of CO in the various tissues [29–31]. In the case of **401** our group has shown that a fast and significant increase in blood carboxyhemoglobin (COHb) levels occurs within five minutes after oral treatment, followed by an accumulation of CO in white adipose tissue at two and six hours [23]. In line with this, our analysis showed that CO prevented the alterations in adipose tissue structure, inflammation and expression of genes involved in fatty acids metabolism induced by a high fat diet (HFD) regime [23].

Thus, targeting the delivery of CO to the adipose tissue may be advantageous to develop new strategies utilizing CO-RMs for the treatment of obesity and metabolic dysfunction. In this context, we found an interesting report showing that biocompatible nanopolysaccharides can be used as efficient carriers to transport anti-inflammatory drugs to adipose tissue [32,33]. In particular, the authors reported that polysaccharides based on biocompatible dextran conjugates linked to anti-inflammatory drugs efficiently distribute to visceral adipose tissue of obese mice, resulting in increased local concentrations and amelioration of tissue function.

In the present study we used a similar approach to synthesize polysaccharides conjugated to CO-RMs and assess their efficacy in obesity. These '**glyco-CORMs**' were obtained by anchoring different numbers of **401** moieties to dextrans (70 and 40 kDa) and were characterized *in vitro* and *in vivo*. Compared to **401**, we show that glyco-CORMs possess an enhanced ability to deliver CO to cells and exert similar anti-obesity and positive metabolic effects in mice subjected to HFD.

2. Results and discussion

2.1. Synthesis of glyco-CORMs

We tested several strategies to achieve the grafting of manganese carbonyls on dextrans with molecular weight of 70 kDa (D70) and 40 kDa (D40). Converting hydroxy groups of dextrans into dithiocarbonate salts by reaction with carbon disulfide in the presence of base, yielded modified polysaccharides that revealed poor ligands of carbonyl manganese complexes such as CORM-401 (**401**). The conjugation of **401** to dextran by esterification in the presence of coupling reagents such as 1-Ethyl-3-(3-dimethylaminopropyl)carbodiimide (EDC; PubMed CID: 15908) or carbonyldiimidazole (CDI) also gave unsatisfactory results. In both cases, the observed lack of reactivity was attributed to the steric hindrance between the polysaccharide and the metal carbonyl complex. To minimize unfavorable interactions, an alternative strategy consisted in the synthesis of a CO-RM containing piperazine [34,35], the latter moiety offering the possibility to both connect and space the two entities. The reaction of piperazine with carbon disulfide in methanol (MeOH; PubMed CID: 887) yielded almost quantitatively the carbamate **1** [36], suitable for complexation with manganese pentacarbonyl bromide ($[MnBr(CO)_5]$; PubMed CID: 10978692) in dichloromethane (DCM; PubMed CID: 6344). The resulting complex **2** was isolated in an overall yield of 91 % under the form of a stable bromohydrate (see Scheme 1). Complex **2** is thus a modified **401** that maintains the ability to release CO (Fig. S1) *in vitro* (cuvette). Prior to conjugation, dextrans D70 and D40 were activated as previously described by CDI in dimethyl sulfoxide (DMSO; PubMed CID: 679) to give, respectively, the two series of polysaccharides **3** and **4** [37,38]. Reactions proceeded in high yields ($>$ 95 %) and with a good control of the number of modified glucose units per polymer chain.

Conjugation of complex **2** with activated dextrans **3a–d** and **4a–d** proceeded in ethanol (EtOH; PubMed CID: 174) in the presence of triethylamine (NEt_3; PubMed CID: 8471). By simply adjusting the quantity of CDI introduced in the reaction mixture, activated dextrans were obtained with approximately 25 % (**a**), 50 % (**b**), 75 % (**c**) and 100 % (**d**) of modified glucose units with carbonyls (complex **2**) per polymer chain (τ, *vide infra*). After reaction, imidazole and unreacted complex **2** were removed by centrifugal ultrafiltration and the crudes were washed with diethyl ether (Et_2O; PubMed CID: 3283). Expected series of glyco-CORMs **5a–d** and **6a–d** were obtained in quite satisfactory yields ($\geq$ 73 %) under the form of amorphous solids that could be stored for months in the dark at 4 °C or below.

2.2. glyco-CORMs release CO in vitro in cuvette and deliver CO to cultured cells

In contrast to **401**, glyco-CORMs were insoluble in DPBS and were thus solubilized in DMSO for testing their ability to release CO *in vitro* in a cuvette (spectrophotometric assay) and in cells in culture (hemoCD1 assay). However, at the concentrations tested, some precipitate appeared over time in the cuvette experiments and in the presence of cells (Fig. S2). When added to a cuvette in the presence of excess concentrations of the CO scavenger hemoCD1 [23,39], all glyco-CORMs showed a significant time-dependent CO release, as shown in Fig. 1A-B. An example of the spectra obtained when glyco-CORM **6b** was added to hemoCD1 is reported in Fig. S3. From the spectra it can be appreciated that the absorbance peak of hemoCD1 shifts from 434 nm (deoxy-hemoCD1) to 422 nm (CO-hemoCD1) over time as the CO released from **6b** binds to the porphyrin-cyclodextrin complex (Fig. S3). The table in Fig. 1 reports the loading in Mn, the total carried CO and the measured CO release from the glyco-CORMs synthesized. The table highlights that the total carried CO (mol/mol of compound) is superior to the actual CO released in cuvette. In fact, glyco-CORMs showed decreasing efficacies with increased manganese tetracarbonyl loading. With the notable exception of **5a**, this trend is observed for the D70-derived glyco-CORMs but not as markedly as with glyco-CORMs **6a–d**. Although this trend remains unclear, it cannot be excluded that it is related to the behavior of the modified polysaccharides in solution and/or to their interaction with the hemoCD1 probe itself. When pre-adipocytes and adipocytes were treated with glyco-CORMs in DMSO, a significant CO accumulation was observed after 3 h (Fig. 1C-D). Intracellular CO increased proportionally to the percentage of metal carbonyl loading of the glyco-CORMs with compound **5a** (25 % loading) causing a lower accumulation of CO than **5b** (50 % loading), and **5b** causing less CO accumulation in cells than **5c** (75 % loading) and so on.

We note that CO levels were higher in cells exposed to 0.5 μM glyco-CORMs compared to 50 μM **401** and that, predictably, no increase in CO was detected in cells treated with the negative control dextran D70 (Fig. 1C-D). We performed additional experiments to confirm that the Mn loading determined the amount of CO accumulated in cells (Fig. S4).

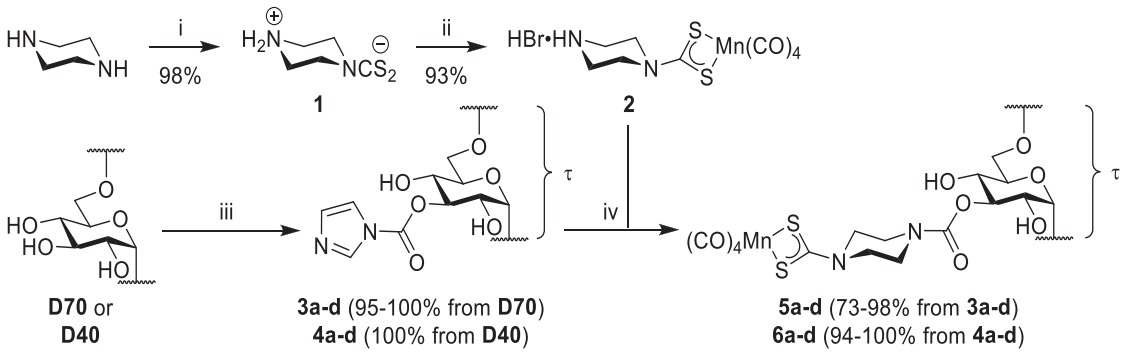

conditions : (i) CS_2, MeOH, r.t., 0.5 h; (ii) $MnBr(CO)_5$, DCM, reflux, Ar, 4 h; (iii) CDI (τ + 0.1 equiv), DMSO, r.t., 18 h; (iv) **2** (τ + 0.1 equiv), NEt_3 (τ + 0.1 equiv), EtOH, 45 °C, Ar, 18 h. **a**, τ ≈ 25%; **b**, τ ≈ 50%; **c**, τ ≈ 75%; **d**, τ ≈ 100%.

Scheme 1. Schematic protocol for the synthesis of glyco-CORMs (see text for details). The resulting modified dextrans D70 (compounds **5a–d**) and D40 (compounds **6a–d**) were grafted with the **401** moiety (complex **2**) leading to different degrees of conjugation: 25 % (**5a** and **6a**), 50 % (**5b** and **6b**), 75 % (**5c** and **6c**) and 100 % (**5d** and **6d**).

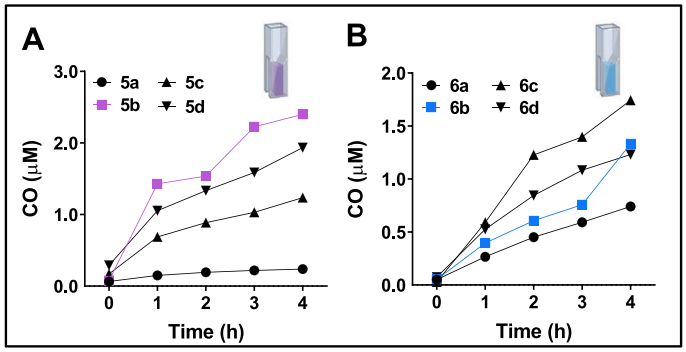

Compound (in DMSO)	5a	5b	5c	5d	6a	6b	6c	6d
Loading in [Mn] (%)	24	48	66	94	19	51	75	90
Total carried CO (mol of CO/ mol of compound)	415	829	1140	1624	188	504	741	889
Measured CO released (mol of CO/ mol of compound)	59	600	309	484	185	351	496	308

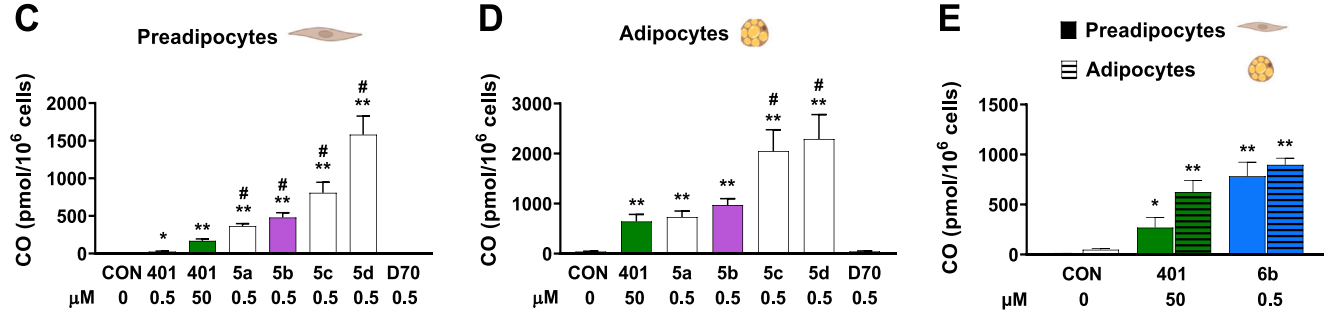

Fig. 1. Glyco-CORMs 5a-d and 6a-d efficiently release CO in a time-dependent manner in cuvette and cells *in vitro*. The release of CO from compounds **5a–d** (A) and **6a–d** (B) (stock solutions prepared in DMSO) was assessed spectrophotometrically over time in cuvette using a solution containing the CO scavenger hemoCD1 (see Experimental Section). The corresponding tabular column provides information on the loading of Mn-carbonyl, the amount of total carried CO and CO released from each compound. Intracellular CO accumulation was assessed in pre-adipocytes (C) and adipocytes (D) after incubation for 3 h with various glyco-CORMs or dextran 70 (D70, negative control). A comparison between **401** (50 μM) and glyco-CORM **6b** (0.5 μM) on their ability to release CO to these two cell types is also shown (E). Data are represented as mean ± SEM ($n = 3$), where $^{*}P < 0.05$ and $^{**}P < 0.01$ compared to control (CON); $^{\#}P < 0.05$ compared to **401**.

Because **5a**, **5b**, **5c** and **5d** exhibited a loading of Mn of 25 %, 50 %, 75 % and 100 %, respectively, we incubated pre-adipocytes with all the compounds at 0.5 μM as well as **5b** at 0.25 μM concentration (half of 0.5 μM), **5c** at 0.17 μM (one third of 0.5 μM) and **5d** at 0.125 μM (one fourth of 0.5 μM). Using this approach, we expected to find that **5b** at 0.25 μM, **5c** at 0.17 μM and **5d** at 0.125 μM would cause an intracellular CO accumulation similar to that of **5a** at 0.5 μM. This was indeed the case, as shown in Fig. S4. These results contrast with the data obtained in cuvette as in cells we found a good a correlation between intracellular CO levels and the percentage loading of glyco-CORMs. It is likely that the experimental approach used to measure CO in cells explains this difference: in fact, cells were incubated with the compounds and washed thoroughly at the end of the treatment, followed by addition of hemoCD1 for detection of CO. Under these conditions hemoCD1 could interact directly with the CO accumulated in cells rather than with glyco-CORMs in solution, which was instead the situation for the experiments in cuvette described above. Importantly, we also observed that CO accumulated intracellularly was generally higher in adipocytes compared to pre-adipocytes after exposure to the compounds (Fig. 1C-E). In additional experiments measuring the accumulation of CO over time we demonstrated a very similar trend using **401**. Fig. S5 shows that in pre-adipocytes CO accumulated in the early hours (1 and 3 h) after **401** exposure followed by a decrease of CO content at 6, 24 and 48 h. Conversely, in immature and mature adipocytes CO accumulated in the

early time points and its levels remained elevated until the end of the experiment. We postulate that this effect is due to an increased sequestration of CO caused by the high lipid content of adipocytes and/or a decreased liberation of CO back into the extracellular milieu once CO is trapped in adipocytes [40]. Finally, when pre-adipocytes were exposed to **5a**, **5b**, **5d** and **401** for 3 h or 24 h we found only a mild reduction in cell viability in the case of **5b** and **5d** (Fig. S6), indicating a good tolerance of cells to the compounds over time.

We reported previously that CO liberated by **401** modulates cellular bioenergetics in different cell types [41,42] and when tested in adipocytes we found that **401** increased mitochondrial oxygen consumption rate (OCR) due to an uncoupling effect [23]. We further showed that this effect stimulated glycolysis and enhanced adipose tissue insulin sensitivity, uncovering an important mechanism by which **401** exerts beneficial actions against obesity-mediated metabolic dysfunction. We wondered if glyco-CORMs would similarly affect adipocyte bioenergetics. Therefore, we performed real-time measurements of changes in metabolism using a Seahorse analyzer in adipocytes treated with compounds **5b** and **6b**. For these experiments, **401** was used as the reference compound at 50 μM, a concentration previously reported in our studies *in vitro* [23,42], while **5b** and **6b** were used at 0.5 μM due to their strong ability to deliver CO to cells. To our surprise, neither **5b** nor **6b** treatment increased OCR, in contrast to the effect elicited by **401** (Figs. S7A-S8A). Notably, **5b** started to decrease OCR from the time of addition to adipocytes (Fig. S7A), thus reducing basal respiration, ATP-linked respiration and other parameters of mitochondrial function (Fig. S7C), while **6b** hardly changed the mitochondrial activity profile compared to control (Figs. S8A-S8C). These results are puzzling but emphasize that the effect of our different compounds on adipocyte bioenergetics cannot be ascribed solely to the intracellular accumulation of CO. It could be argued that the considerable amount of CO delivered by **5b** justifies the significantly depressed respiration due to the known mitochondrial-poisoning effect of CO [20,43,44]. Indeed, in microglia cells for instance, **401** exerts uncoupling activities at 10–50 μM (low CO accumulation) while it inhibits respiration at 200–500 μM (high CO accumulation) [42]. On the other hand, **6b** did not inhibit mitochondrial respiration despite being able to increase intracellular CO accumulation similarly to **5b**. We suggest that the capacity of the compounds to liberate CO in the vicinity of mitochondria may be an important factor determining their modulation of cellular bioenergetics.

2.3. Distribution of CO between adipocytes and macrophages co-cultured in the presence of 401 and 6b

During obesity a remodelling of the adipose tissue occurs, with infiltration of macrophages that become activated and contribute to a pro-inflammatory phenotype [45,46]. We were thus interested in examining the accumulation of CO also in macrophages exposed to glyco-CORMs and compare their behaviour to that of adipocytes. We first showed that both adipocytes and macrophages cultured separately (single culture) exhibited significant CO accumulation 3 h after incubation with 50 μM **401** and 0.5 μM **6b** (Fig. 2A). Intracellular CO levels were much higher in the presence of **6b** even if the compound was used at a concentration 100 times lower than **401**. Adipocytes also appeared to accumulate more CO compared to macrophages when exposed to **401** and **6b**, although the difference between these two compounds was not significant. In additional experiments we then assessed whether the activation state of macrophages could influence CO accumulation. Resting macrophages (MΦ) or macrophages challenged with lipopolysaccharide (LPS) (M1) were incubated with **401** or **6b** and after 3 h we observed a significant CO accumulation with no difference between the inactivated and the activated macrophages (Fig. 2B). These data indicate that macrophages have a similar capacity to uptake CO from **401** or glyco-CORMs compared to adipocytes and that the inflammatory profile of macrophages does not affect CO accumulation during the time of our experiments.

We next performed a series of experiments in a co-culture system of mature adipocytes and macrophages and studied the effect of **401** and **6b** on CO uptake using different setups. In setup 1, adipocytes were grown in 6-well culture plates and macrophages seeded on transwell membranes were placed on top of the wells during the experiment (Fig. 3A). CO-releasing compounds were added to macrophages or adipocytes and CO levels were determined in both cell types. Interestingly, when **401** was added to macrophages (Protocol 1 in Fig. 3A), 68 % of the total measurable CO accumulated in macrophages and 32 % in the underlying adipocytes. In the case of **6b**, 95 % of CO was detected in macrophages and only 5 % in adipocytes (Fig. 3A). Similarly, when adipocytes were treated with **401** (Protocol 2 in Fig. 3A), 65 % of CO accumulated in adipocytes and 35 % in the overhanging macrophages while after exposure to **6b** 96 % of CO was measured in adipocytes and only 4 % in macrophages (Fig. 3A). In setup 2, macrophages were grown in 6-well culture plates and adipocytes were differentiated on transwell membranes that were placed on top of the wells during the experiment (Fig. 3B). Again macrophages or adipocytes were treated with the CO-releasing compounds and CO levels determined in both cell types.

As observed in setup 1, 73 % and 96 % of CO accumulated in adipocytes and 27 % and 4 % of CO in the underlying macrophages when **401** or **6b**, respectively, were added to adipocytes on top (Protocol 3 in Fig. 3B). In protocol 4, macrophages at the bottom exposed to **401** and **6b** exhibited, respectively, 43 % and 95 % CO while 57 % and 5 % CO was detected in adipocytes on top (Fig. 3B).

Altogether, these data indicate that CO levels increase predominantly in the cell type coming in direct contact with the compounds, regardless of whether cells are growing at the top or bottom of the co-culture system. However, a main difference is that treatment with **401** results in approximately one third of the total CO accumulation in the cell type that did not come in direct contact with the compound (with the exception of Protocol 4 in setup 2), while for **6b** the vast majority of

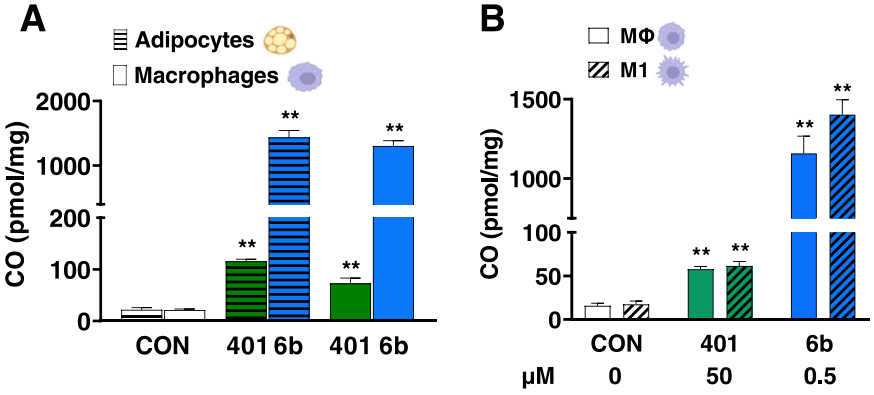

Fig. 2. Comparative effects of 401 and glyco-CORM 6b on their ability to deliver CO to adipocytes and macrophages. Adipocytes and macrophages were treated with either **401** (50 μM) or **6b** (0.5 μM) (stock solutions prepared in DMSO) and intracellular accumulation of CO was measured after 3 h incubation (A). Intracellular CO uptake was also assessed in naïve "inactivated" macrophages (MΦ) or macrophages "activated" with 1 μg/mL LPS (M1) for 24 h prior to incubation with either **401** or **6b** for 3 h (B). Data are represented as mean ± SEM ($n = 3$), where * $P < 0.05$ and * * $P < 0.001$ compared to control (CON).

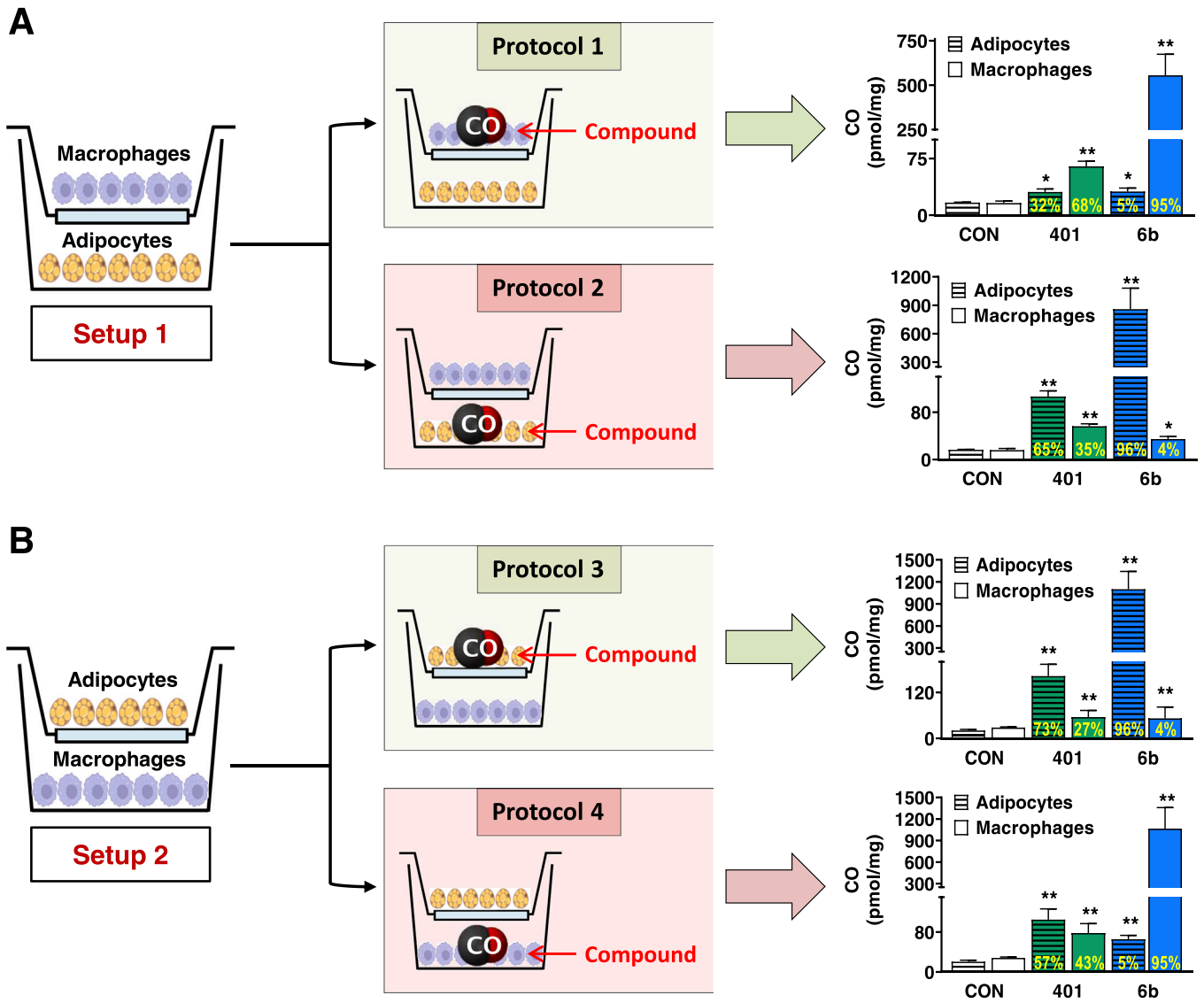

Fig. 3. CO distribution between adipocytes and macrophages co-cultured in the presence of 401 and glyco-CORM 6b. A trans-well co-culture system was used to assess the distribution of CO accumulation between adipocytes and macrophages after treatment with **401** (50 μM) or **6b** (0.5 μM) for 3 h (stock solutions prepared in DMSO). Two different set-ups were used: in setup 1, macrophages were cultured on the insert membrane placed on top while adipocytes were cultured on the bottom wells (A); in setup 2, adipocytes were cultured on top and macrophages on the bottom (B). Within each setup, two different protocols were applied depending on whether **401** or **6b** were incubated in direct contact with the macrophages (Protocols 1 and 4) or adipocytes (Protocols 2 and 3). Data in the bar graphs are represented as mean ± SEM ($n = 3$), where * $P < 0.05$ and * * $P < 0.01$ compared to control cells (CON). The numbers in yellow within each bar graph indicate the distribution of CO (%) between macrophages and adipocytes within each protocol performed.

intracellular CO was found in the cell type that was directly exposed to the compound. Considering that adipocytes and macrophages were separated by the transwell membrane, which has a pore size of 0.4 μm and permits an exchange of soluble molecules [47], it appears that CO and/or the small **401** compound (MW = 343 Da) were able to move more freely into the co-culture environment leading to a more homogeneous distribution of intracellular CO in the two compartments. In contrast, the very high molecular weight of **6b** (MW = 84 kDa) may render the molecule unable to move across the transwell insert, explaining the limited exchange of CO between cells. It is also possible that the different CO distribution is due to the nature of the compounds and a distinct mode of CO delivery between **401** and **6b,** as already suggested by the results obtained in the bioenergetic experiments described above (Figs. S7A-S8A). Finally, the results with **401** using protocol 4 in setup 2, where more CO was measured in adipocytes despite the fact that the compound was added directly to macrophages, could be explained by a propensity of CO and/or **401** given to macrophages to move upwards and by the strong ability of adipocytes to trap CO, as discussed above (see Fig. S5).

2.4. In vitro and in vivo CO release by glyco-CORMs dissolved in a solution containing β-cyclodextrin, polyethylene glycol and poly (N-vinyl-pyrrolidone) (PP formulation)

Because glyco-CORMs had limited solubility in DMSO, we decided to solubilize the compounds in a different solution that would also be suitable for oral administration in mice. For this, a formulation that is commonly used in the clinic to dissolve compounds with low solubility was employed and consisted of polyethylene glycol 400 (1 mL) with the addition of β-cyclodextrin (20 mg) and poly (N-vinyl-pyrrolidone) (50 mg) (see PP formulation in Experimental Section). Dissolving glyco-CORMs in the PP formulation produced a suspension (Fig. S2), in line with the known ability of β-cyclodextrin and the other components of the PP formulation to facilitate the solubility of compounds [48–52]. In

order to assess the ability of glyco-CORMs to deliver CO *in vivo*, lean mice were orally administered with **401** and the **5a–d** and **6a–d** series followed by measurements of COHb over time. Because different numbers of **401** moieties are conjugated to glyco-CORMs, the dose of each glyco-CORM was calculated in order to administer the same amount in moles/liter of conjugated **401** found in 30 mg/kg **401** alone (Table S1). Although **401** elicited the strongest increase in COHb (approximately 3.5 % COHb at 1 and 3 h after administration), all glyco-CORMs also caused a rise in this parameter (Fig. 4A-B). This significant effect was noticeable in the early hours after administration while at 24 h COHb returned to basal values in the case of glyco-CORMs but not **401** treatment. Indeed, COHb was still over 1 % 24 h after **401** administration. Despite the different Mn loading, we could not detect a loading-dependent increase in COHb after glyco-CORMs treatment. Among the **5a–d** series, compound **5b** was the most efficient in increasing COHb; among the **6a–d** series all compounds behaved very similarly (Fig. 4B).

These results are surprising since glyco-CORMs were administered with the same equivalents of CO as in **401** and therefore we expected to obtain the same COHb levels after treatment with all compounds. Therefore, our data suggest that the size of glyco-CORMs as well as the peculiar structure of these compounds reduce their bioavailability and their capacity to release CO *in vivo*, making them less efficient than **401**.

The behavior of compounds **5b** and **6b** in PP formulation was further analyzed *in vitro* as representative D70 and D40 derivatives with the same 50 % loading. Incubation in cuvette with excess concentration of hemoCD1 confirmed that the two compounds (0.02 μM) in the PP formulation released more CO than **401** in a time-dependent manner (Fig. 4C). When pre-adipocytes and adipocytes were exposed to **5b** and **6b**, a significant increase in CO uptake was observed after 3 h, with a very pronounced CO accumulation following incubation with **5b** (Fig. 4D-E). As observed before, CO accumulation in cells after exposure to the compounds at 0.5 μM was higher than that measured with **401** at 50 μM. The effect on cell viability of **5b** and **6b** solubilized in the PP formulation was also studied in both preadipocytes and adipocytes. The results in Fig. S9 show that **5b** was the compound that mostly reduced cell viability of pre-adipocytes and mature adipocytes at 3 and 24 h, possibly due to the high levels of CO achieved in cells in the presence of the compound. Overall, it appears that the PP formulation improved the solubilisation of glyco-CORMs and hence resulted in efficient CO delivery. However, the results *in vitro* (cuvette and cells) emphasize the capacity of glyco-CORMs to liberate significant amounts of CO when coming in direct contact with 'simpler' biological environments while the results *in vivo* indicate that the size and complexity of the molecules diminish their bioavailability and efficacy in terms of CO release in animals.

2.5. CO release and tissue distribution following administration of glyco-CORMs 5b and 6b in obese mice

Because glyco-CORMs were designed to target the adipose tissue, we next measured COHb and CO accumulation in different organs after oral administration of glyco-CORMs (in PP formulation) and **401**. These experiments were performed in obese mice obtained after feeding a high

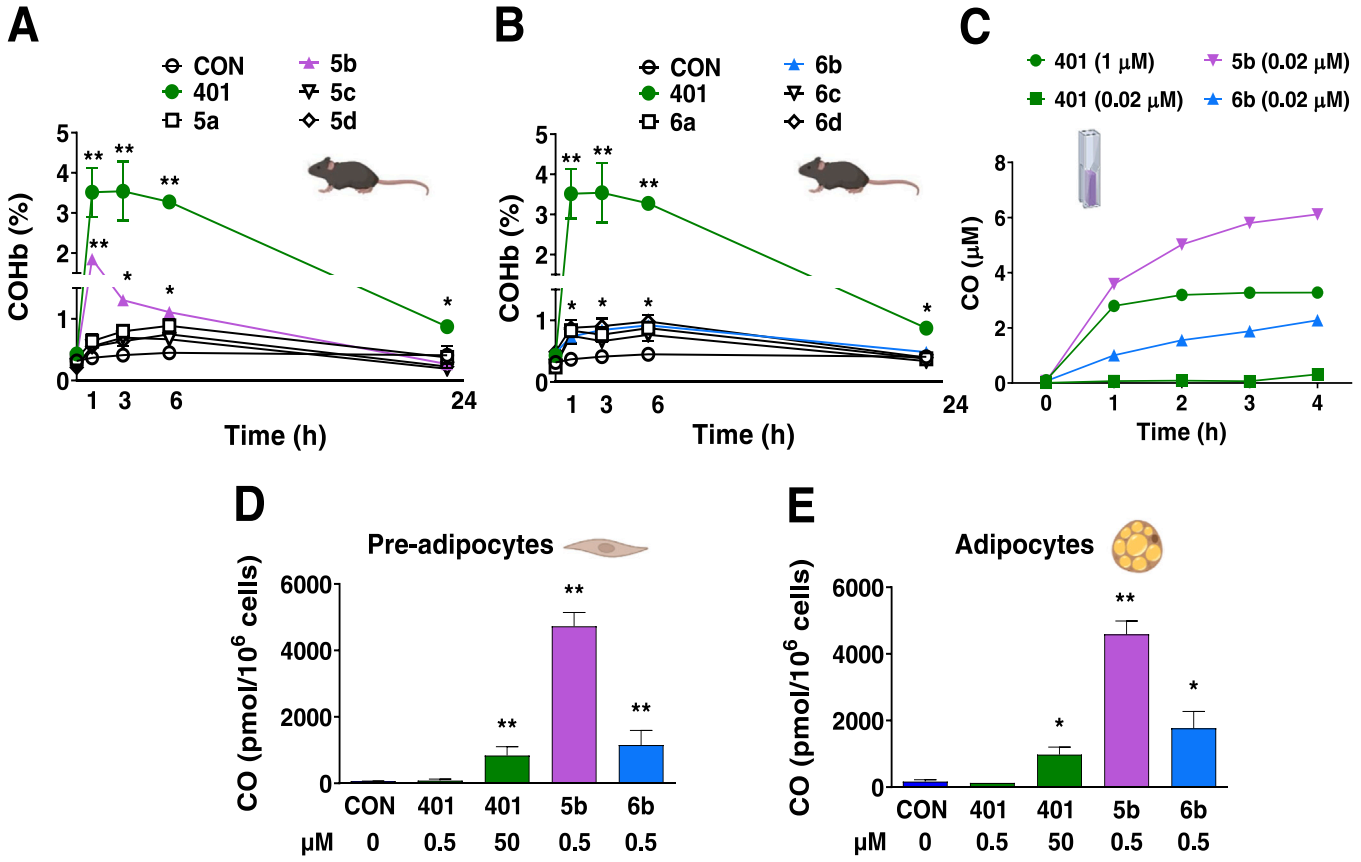

Fig. 4. Effect of glyco-CORMs solubilized in PP formulation on their ability to deliver CO *in vivo* and *in vitro*. A time-course of CO delivery from glyco-CORMs **5a–d** (A) and **6a–d** (B) in comparison with **401** was performed in lean mice by assessing changes in blood COHb levels over time following oral administration of each compound solubilized in PP formulation (see Experimental Section for details). CO release from 401 (1 μM and 0.02 μM) and glyco-CORMs **5b** (0.02 μM) and **6b** (0.02 μM) was also assessed spectrophotometrically over time in a cuvette using a solution containing the CO scavenger hemoCD1. Intracellular accumulation of CO was determined in pre-adipocytes (D) and mature adipocytes (E) after 3 h incubation with **401**, glyco-CORMs **5b** or **6b** solubilized in PP formulation. Results are expressed as mean ± SEM ($n = 3$), where * $P < 0.05$ and * * $P < 0.01$ compared to control groups (CON).

fat diet (HFD) for 8 weeks in order to have a significant amount of fat tissue (see scheme in Fig. 5A), which is normally present in small quantities in young lean mice. The curve of COHb levels in obese mice (Fig. 5B) was similar to that obtained in lean mice (Fig. 4A) for **401** although values were slightly lower for compounds **5b** and **6b**. The levels of CO were significantly elevated in the liver (Fig. 5C), kidney (Fig. 5D), adipose tissue (Fig. 5E, non significant), pancreas (Fig. 5F), small intestine (Fig. 5G), colon (Fig. 5H) and faeces (Fig. 5I) 6 h after administration of **401** and, to a smaller extent, **5b** (Fig. 5C-I). Administration of **6b** resulted in a modest increase in CO levels in the faeces (Fig. 5I). Various parameters influence the adsorption, distribution, metabolism and excretion of polysaccharides within the biological system [53,54]. The differences in molecular weight of **401**, **5b** and **6b** may govern the transition of the compounds through the gastrointestinal tract [55,56] and, in the case of our molecules that are formed by dextrans conjugated with CO-RMs, affect the release and distribution of CO.

The presence of different proteins with more or less ability to bind CO in each organ will also strongly influence the delivery and accumulation of CO in the organism. In addition, the high CO levels in the liver and kidney is in accordance with the putative role of these two organs in metabolism and excretion of drugs [57]. Although these measurements were conducted after acute administration of the compounds, our previous report showed that prolonged treatment with **401** during HFD in mice leads to reduced weight gain and improved insulin and glucose metabolism, including a decrease in liver steatosis [23]. This suggests that temporal accumulation of CO in the liver (and other organs) exerts beneficial effects during HFD. Our experiments did not confirm that **5b** and **6b** could preferentially deliver CO to the adipose tissue after oral administration and similar results were obtained if the compounds were injected intraperitoneally (data not shown). This is in contrast with findings from Ma and co-workers, who reported that nanoscale dextran conjugates carrying an anti-inflammatory drug given intraperitoneally (but not intravenously) led to strong distribution of the compounds in the visceral adipose tissue after acute treatment [33]. The fact that a different conjugation strategy was used in the present work to anchor manganese carbonyls to the polysaccharides may partially explain the lack of CO accumulation in the adipose tissue after acute treatment with glycol-CORMs.

2.6. Glyco-CORM 6b prevents weight gain and improves metabolism in HFD fed mice

Administration of glyco-CORMs solubilized in the PP formulation resulted in transient loose stools, as shown previously [58]. Hence, although the PP formulation can be used for acute studies, we decided that its utilization would be unsuitable for long-term administration in animals fed with HFD, since one important objective of our study was to determine if the compounds could prevent HFD-induced weight gain. Thus, the compounds were solubilized in a mixture of DMSO and sunflower oil and we confirmed using hemoCD1 that also in this solution

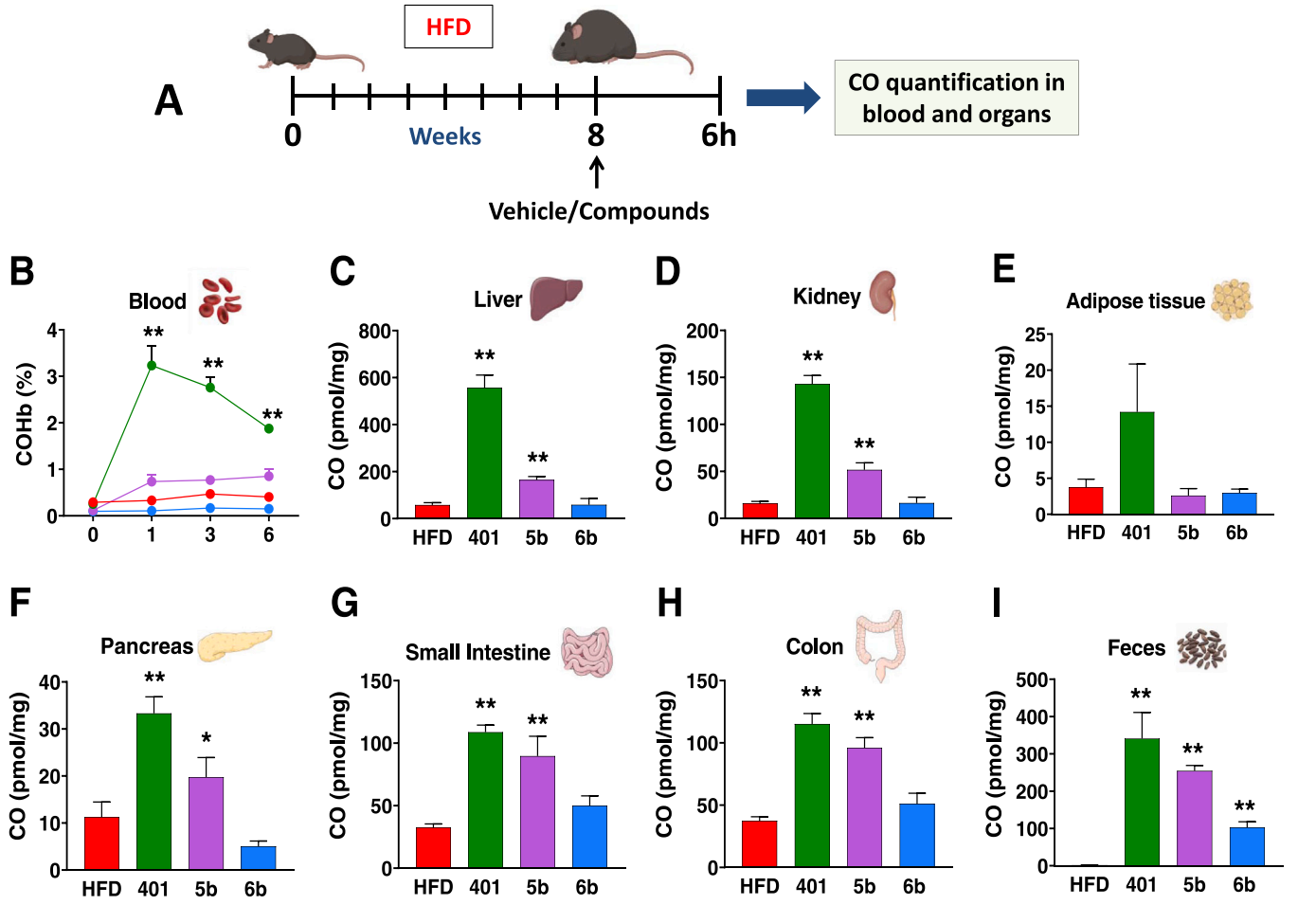

Fig. 5. CO delivery and tissue distribution following acute administration of glyco-CORMs 5b and 6b in obese mice. Schematic representation of the protocol used (A). After mice were fed a high fat diet for 8 weeks, they were treated with an oral administration of either vehicle (CON), **401** (30 mg/kg), glyco-CORM **5b** (62 mg/kg) or **6b** (60 mg/kg) solubilized in the PP formulation. Blood, organs and faeces were collected 6 h after treatment to assess the levels and distribution of CO. CO was assessed in blood by measuring COHb over time (B) as well as in liver (C), kidney (D), adipose tissue (E), pancreas (F), small intestine (G), colon (H) and faeces (I) using the hemoCDs assay. Results are expressed as mean ± SEM ($n = 5$), where * $P < 0.05$ and * * $P < 0.01$ compared to control groups (CON).

they release CO (Fig. S10). Oral administration of equivalent doses of **5b** and **6b** in mice gave rise to a significant increase in circulating COHb compared to control in the first 6 h after gavage (Fig. S11). To decide which compound to use for the long-term HFD regime experiments, we took into consideration that **5b** showed a more pronounced reduction in cell viability (Fig. S9) and a profound inhibition of mitochondrial respiration (Fig. S7) compared to **6b**, which was well tolerated by cells and did not exert mitochondrial dysfunction (Fig. S8). Thus, we chose to study the effect of **6b** against obesity in mice fed a HFD for 8 weeks (see scheme in Fig. 6A).

As shown in Fig. 6B, at the end of the 8 weeks treatment and following the last dose of **6b** and **401**, we measured a significant increase in COHb up to 6 h (time of sacrifice). These results demonstrate that a transient rise in COHb levels is achievable after each administration of **6b** and are consistent with previous results obtained with **401** (this article and [23]). Assessment of different metabolic parameters also suggested a positive role of **6b**. Body weight gain in mice under HFD was significantly reduced by both **6b** and **401** (Fig. 6C). Compounds **6b** and **401** also significantly improved insulin sensitivity (ITT, Fig. 6D) and glucose tolerance (GTT, Fig. 6E) as evident from the decrease in glucose excursion. After administration of **6b** and **401** CO levels were elevated at 6 and 24 h in the faeces of animals (Fig. 6F). CO accumulation in the

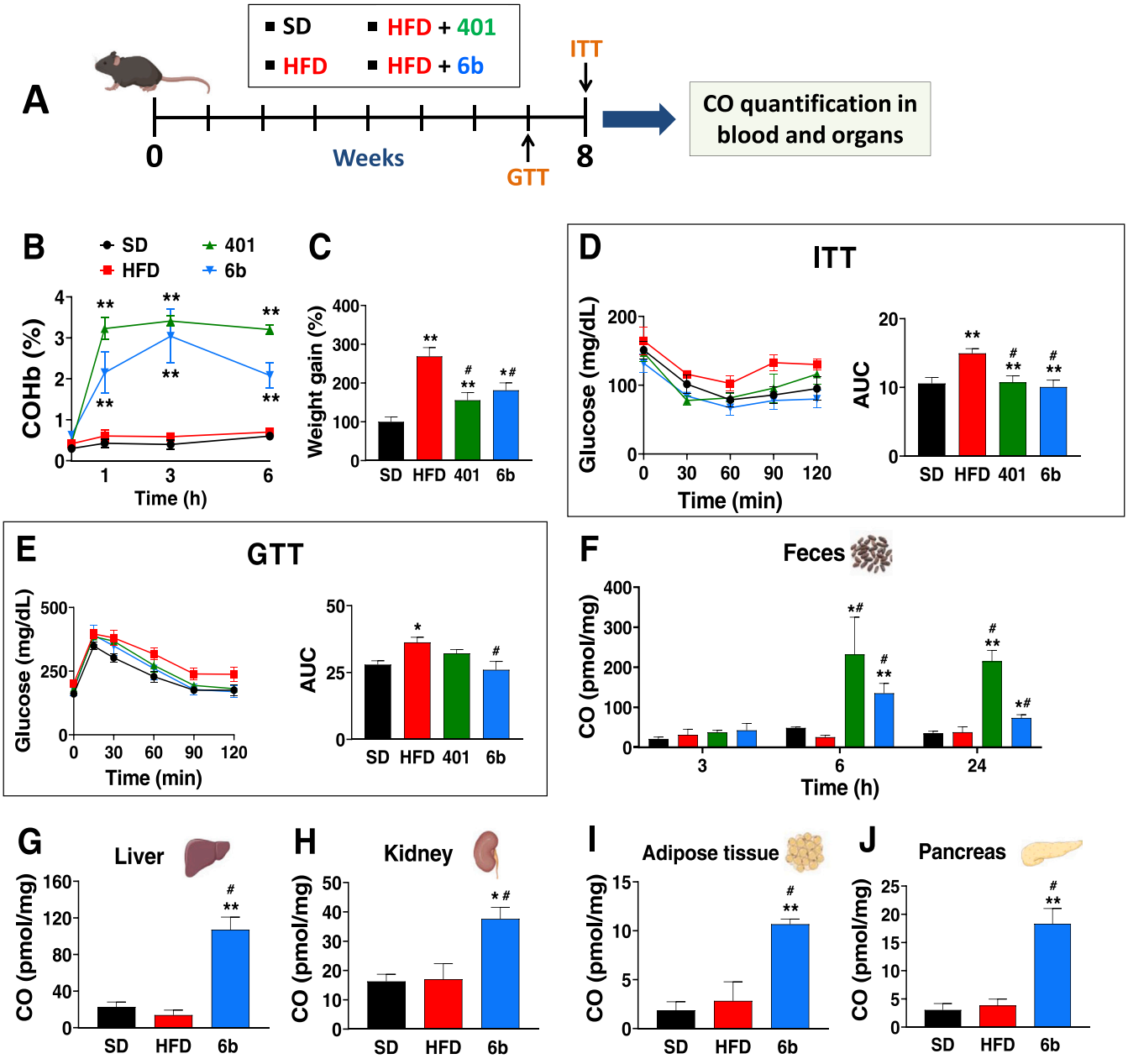

Fig. 6. Repetitive administration of glyco-CORM 6b ameliorates insulin sensitivity and prevents weight gain in mice fed a high fat diet (HFD). Mice were fed either a standard diet (SD) or a HFD for 8 weeks. In two additional groups, mice on HDF were treated with either CORM-401 (30 mg/kg in PBS) or glyco-CORM 6b (60 mg/kg in DMSO-sunflower oil) administered orally 3 times a week for 8 weeks before assessing different parameters (A). A time-course of blood COHb levels was assessed at end of the 8 weeks treatment in each group following administration of the compounds (B). Body weight gain was determined following the treatments (C) alongside the assessment of metabolic parameters by performing insulin tolerance (ITT, D) and glucose tolerance (GTT, E) tests (see Experimental Section for details). The distribution of CO was analyzed in different organs collected at the end of the 8 weeks treatment and these included faeces (F), liver (G), kidney (H), adipose tissue (I) and pancreas (J). Results are expressed as mean ± SEM ($n = 6/7$), where * $P < 0.05$ and * * $P < 0.01$ compared to mice fed a SD; $^{\#}P < 0.05$ compared to mice fed a HFD. AUC, area under the curve.

liver, kidney, adipose tissue and pancreas collected after 8 weeks of treatment with HFD+**6b** was also higher compared to animals receiving the standard diet or HFD alone, indicating an effective delivery of CO by **6b** to the organism (Fig. 6G-6J). The significant increase in CO content in adipose tissue and pancreas suggests that CO from **6b** or the compound itself reach body compartments outside the gastrointestinal tract and is in line with the improvements in overall metabolism exerted by the compound. This may also indicate an improved glucose uptake in peripheral tissues caused by the release CO since this gas acts as a ubiquitous secondary signalling molecule as observed in our previous work [23]. Interestingly, these data are in contrast to the findings presented in Fig. 5, showing that acute administration of **6b** in obese mice did not lead to CO accumulation in liver, kidney, adipose tissue and pancreas. Therefore, we deduce that CO levels can be markedly increased in tissues only after cumulative administrations in animals with **6b**. Conversely, a single acute treatment of **6b** is not sufficient to increase CO levels in organs.

3. Conclusion

In summary, novel derivatives of CO carriers were synthesized starting from the conjugation of **401** onto dextrans and leading to the generation of glyco-CORMs possessing multiple functionalized CO-RMs. Our results show that these compounds have a high ability to deliver CO to cells and that glyco-CORM **6b** can counteract negative effects elicited by a HFD regime in mice, with reduction in body weight gain and amelioration of the metabolic profile similar to those obtained with **401**. Administration of glyco-CORMs *in vivo* did not lead to specific accumulation of CO in the adipose tissue, which was one of the desirable features envisaged when designing polysaccharide-bound CO-RMs. This strategy was inspired by articles from Ma and Prabhu [32,33], who developed dextran nanocarriers for the targeted delivery of anti-inflammatory drugs to the macrophages of adipose tissue during obesity. However, although the dextran nanocarriers favoured the targeting of the adipose tissue, there was still uptake of the compounds in the liver and the spleen [33], indicating the difficulty in vehiculating substances to a specific organ/tissue when administering drugs in a systemic manner, which was the case for the glyco-CORMs synthesized in the present work. Nevertheless, it was interesting to observe in our *in vitro* experiments that adipocytes exposed to our compounds have a greater capacity than other cell types to accumulate and store CO, which may be a consequence of the ability of fat cells to store organic chemicals for a long time [59] and the high lipophilicity of CO/CO-RMs.

Importantly, our study reports for the first time the distribution of CO in the organism after oral treatment of mice with **401** and glyco-CORMs, highlighting a significant accumulation of CO in several organs and that liver, kidney and faeces contained the highest levels of CO 6 h after treatment with the compounds. Alongside the determination of blood COHb, the results of these measurements allowed us to gain useful information about the pharmacokinetics of CO-RMs. For example, the facts that the pancreas also showed a marked increase in CO levels in obese mice and that it is a central organ in metabolism suggest interesting avenues for future studies aimed at deciphering the beneficial action of CO against obesity and glucose intolerance.

Finally, the present work underlines our substantial effort in investigating different solvents that could improve the solubility of glyco-CORMs and are suitable for oral administration in humans (PP formulation). Therefore, in addition to designing new chemical entities that serve as CO carriers *in vivo*, the optimization of formulations that can maximize the pharmacological effects of CO in a given pre-clinical model is equally relevant for the further development of CO-based therapeutics [60].

4. Experimental section

4.1. Reagents for biological studies

Stock solutions of **401** (10 mM) were prepared by solubilizing the compound in Dulbecco's phosphate buffer solution (DPBS, pH=7.4). glyco-CORMs were solubilized either in 1) DMSO (Sigma-Aldrich), 2) in-house formulation consisting of β-cyclodextrin, polyethylene glycol 400, and poly (N-vinyl-pyrrolidone) (PP formulation) [48–52] or 3) a mixture of DMSO (3 %) and sunflower oil previously used by our group to solubilize other types of CO-RMs derivatives [61]. Stock solutions were stored at − 20 °C until use and animal treatments were performed with freshly prepared stocks. DPBS, DMEM, newborn calf serum, fetal bovine serum (FBS), penicillin/streptomycin, and trypsin were purchased from Life Technologies (Saint Aubin, France). Pyruvate, isobutylmethylxanthine (IBMX), and human insulin solution were obtained from Merck (France). All other analytical grade reagents were obtained from Sigma-Aldrich.

4.2. Cell culture

3T3-L1 preadipocytes (088SPL1F, Tebu-Bio, France) were cultured in DMEM medium (4.5 g/L glucose) supplemented with 10 % newborn calf serum and antibiotics, in an atmosphere of 5 % CO_2 at 37 °C. Differentiation into adipocytes was stimulated in a medium containing 10 % FBS, 3-isobutyl-1-methylxanthine (IBMX, 500 μM), dexamethasone (250 nM), and insulin (175 nM) for two days (immature adipocytes), followed by two days of treatment in DMEM with FBS and insulin (175 nM) to obtain mature adipocytes. Cells were then maintained in DMEM with 10 % FBS only until the day of the experiment. Raw 264.7 murine macrophages (ATCC, UK) were grown in DMEM containing 4.5 g/L glucose and Glutamax supplemented with 10 % FBS (Life Technologies).

4.3. Assays for detection of CO in cuvette and cells in culture

Kinetics of CO release from glyco-CORMs were determined in cuvette using the specific CO scavenger hemoCD1 [43]. HemoCD1 was synthesized as previously described [62]. Briefly, hemoCD1 and sodium dithionite ($Na_2S_2O_4$, 1–2 mg) were added to a cuvette containing DPBS. Glyco-CORMs (0.5 μM) or **401** (50 μM) were added to the cuvette and absorbance was measured between 400 nm and 500 nm at different time points using a UV-Vis spectrophotometer (JASCO V-730). Intracellular CO accumulation after incubation with the compounds was also investigated using pre-adipocytes, adipocytes, and naïve macrophages (MΦ) or pro-inflammatory macrophages (M1) pre-treated for 24 h with 1 μg/mL lipopolysaccharide (LPS) [23,42]. Briefly, after 3 h incubation with compounds cells were gently washed and scraped in 1 mL DPBS. HemoCD1 and sodium dithionite ($Na_2S_2O_4$, 1–2 mg) were added and samples were collected, sonicated and centrifuged to remove cell debris. The supernatant was filtered through a 0.22 μm filter before measurements of spectra using a spectrophotometer [39].

4.4. Cell viability

3T3-L1 preadipocytes or differentiated adipocytes in a 96 well plate were incubated with either **401** (50 μM) or glyco-CORMs (0.5 μM) for 3 h or 24 h. The effects of the compounds on viability were evaluated using the MTT (3-(4,5-dimethyl-2-thiazolyl)-2,5-diphenyl-2H-tetrazolium bromide) assay as previously described [63].

4.5. Cellular bioenergetics

The bioenergetic profile of differentiated 3T3-L1 adipocytes was determined using a Seahorse XF24 Analyzer (Agilent Technologies, Santa Clara, CA, USA), which measures mitochondrial respiration and

glycolysis, as previously described [23]. Glyco-CORMs **5b** and **6b** (0.5 μM) and **401** (50 μM) were added prior to performing a MitoStress test, consisting of sequential additions of 1 μg/mL oligomycin, 0.63 μM carbonyl cyanide 4-(trifluoromethoxy) phenylhydrazone (FCCP; PubMed CID: 132276760) and 1 μM rotenone (PubMed CID: 6758) and antimycin A (PubMed CID: 14957). Different parameters, including ATP-dependent respiration, proton leak, and maximal respiratory capacity, were calculated from the profile of mitochondrial respiration.

4.6. CO accumulation in adipocytes and macrophages in a co-culture system

The uptake of CO from **401** and **6b** was assessed in a co-culture system using 3T3-L1-differentiated adipocytes and RAW 264.7 macrophages. Two different co-culture systems were designed as follows: in setup 1 3T3-L1 pre-adipocytes were cultured and differentiated into adipocytes in a 6-well plate while macrophages were seeded on transwell membranes with pore size 0.4 μm (CORNING, France) (Fig. 5D); in setup 2 3T3-L1 cells were cultured and differentiated on the transwell membranes and macrophages were grown in a 6-well plate (Fig. 5E). Adipocytes and macrophages were grown separately until the day of the experiment when the cells were co-cultured by inserting the transwell membranes onto the 6-well plate. To assess whether adipocytes or macrophages preferentially accumulate CO, **401** (50 μM) or **6b** (0.5 μM) was added either to the adipocytes or the macrophages for 3 h in both setups. Intracellular CO levels were quantified using hemoCD1 as described above. Intracellular CO levels were normalized to the protein content of the cells.

4.7. Protein quantification assay

Protein concentration was analyzed using the Pierce BCA protein assay kit according to the manufacturer's instructions (Thermo Fischer Scientific, USA).

4.8. Animal studies

Eight-week-old C57BL6J mice were purchased from Janvier (France) and housed under controlled temperature (21 °C ± 1 °C), hygrometry (60 % ± 10 %), and lighting conditions (12 h light cycle). All animal procedures were conducted according to a license and care of animals following INSERM guidelines. Animals were acclimatized in the animal facility for 1 week before use for the experiments. In the first protocol, lean mice were used to test the pharmacokinetics of CO release from glyco-CORMs (n = 3 per group). Animals were randomly assigned to different treatments or control groups and, whenever possible, samples were blindly analyzed in order to minimize bias. Mice were orally administered equivalent doses of glyco-CORMs (PP formulation or DMSO and sunflower oil) and blood was collected from the tail vein at different time points for the measurement of carboxyhemoglobin (COHb). Equivalent doses were calculated based on glyco-CORMs molecular weight and the number of CO-RMs attached (Table S1). The compound **401** was administered orally at 30 mg/kg as described before [23]. In a second protocol, *in vivo* pharmacokinetics of glyco-CORMs were assessed in obese mice (n = 5 per group). Mice were fed a high-fat diet (HFD, Purified Diet 230 HF, Research Diets, USA) for 8 weeks to induce obesity and fat accumulation. On the day of the experiment, animals were administered **401** or glyco-CORMs (both in PP formulation) at an equivalent dose (Table S1), and 6 h after administration organs were collected after flushing with 0.9 % saline *via* transcardial perfusion. The organs were immediately snap frozen in liquid nitrogen and stored at − 80 °C until CO measurements. In a third protocol, the effect of long-term administration of compound **6b**, solubilized in DMSO and sunflower oil, was assessed in mouse models of obesity (n = 5–7 per group). Mice fed with HFD received **401** (30 mg/kg) or **6b** (60 mg/kg) orally thrice a week for 8 weeks. Control mice were fed a standard diet and a third group received HFD with vehicle (DMSO and sunflower oil). Body weight was monitored every week and CO levels in the faeces and COHb were determined at week 3 and week 8, respectively. At the end of the protocol, mice were sacrificed and all organs were snap frozen and stored at − 80 °C prior to CO measurements. In separate experiments, CO accumulation was also examined in adipose tissue 6 h after intra-peritoneal administration of **6b** solubilized in DMSO and sunflower oil (60 mg/kg).

4.9. Fasting glucose and insulin tolerance tests

Whole-body glucose tolerance (GTT) and insulin sensitivity tests (ITT) were performed at weeks 7 and 8 after a 6 h fast in mice from the third protocol. Blood glucose was measured before administration of glucose or insulin at 0 h using a freestyle optimum Neo H glucose monitor (Abbott, UK). Mice were then administered glucose (1.5 g/kg) or insulin (0.3 UI/kg) by intraperitoneal injection. Blood glucose was measured at 15, 30, 60, 90, and 120 min after injection. The area under the curve for the glucose excursion was calculated using Graphpad Prism.

4.10. Quantification of carboxy-hemoglobin (COHb) in circulation

Levels of COHb in blood were measured as previously described by our laboratory following a protocol developed by Rokdey and colleagues [23,64,65].

4.11. Quantification of CO in tissues

CO levels were measured in organs collected from perfused mice after administration of **401** and glyco-CORMs as reported by Mao and collaborators [43]. Briefly, snap-frozen tissues were weighed and homogenized in DPBS using Qiagen tissue lyserII (Qiagen, UK). Homogenates were added to a solution containing hemoCD1 (2–10 μM) with $Na_2S_2O_4$ (1–2 mg) and vortexed. Samples were then centrifuged at 12, 700 rpm for 15 min, the supernatant was transferred to fresh tubes and $Na_2S_2O_4$ (1–2 mg) was added again to maintain hemoCD1 in the deoxy state. After a second centrifugation, the supernatant was passed through a 0.22 μm filter prior to measurement of absorbance between 400 and 500 nm using a UV–vis spectrophotometer.

4.12. Statistics

Data are expressed as mean ± SEM. Statistical analyses were performed using the unpaired 2-tailed Student's t-test or 2-way ANOVA with Fisher multiple comparison test. Results were considered significant if the *P* value was less than 0.05.

4.13. Chemistry: general procedure

Manganese pentacarbonyl bromide and CORM-401 (**401**) were synthesized as previously described [22,66]. Dextran from *Leuconostoc spp.* was purchased from Sigma-Aldrich with average molecular weights of 70 and 40 kDa. Dimanganese decacarbonyl was purchased from Strem. Acetone was purchased from Acros Organic and DMSO from Alfa Aesar. Other solvents were purchased from Carlo Erba. Water was freshly distilled prior to any reaction or washing. Reagents were purchased from Sigma-Aldrich and were used without further purification. All reactions were performed under a dry anaerobic argon atmosphere. Reactions involving manganese carbonyls were carried out in the dark. ^{1}H and ^{13}C nuclear magnetic resonance (NMR) spectra for characterization of new compounds were collected in anhydrous DMSO-d_6 or DMF-d_7 (from Eurisotop) at 293 K and were recorded on a Bruker Avance-II 400 MHz spectrometer. Chemical shifts are reported in parts per million (ppm) and referenced to the residual solvent peaks: δ_{1H}(DMSO-d_6) = 2.50 ppm, δ_{13C}(DMSO-d_6) = 39.5 ppm, $\delta_{1\,H}$(DMF-d_7)

= 8.03, 2.92 and 2.75 ppm, $\delta_{13\ C}$(DMF-d_7) = 163.2, 34.9 and 29.8 ppm. Splitting patterns are indicated as follows: s, singlet; bs, broad singlet; d, doublet; t, triplet; q, quartet; m, multiplet. Spectra were processed and analysed with MestreNova software. Elucidation of the chemical structures was based on ^{1}H, ^{13}C, COSY and HSQC experiments for compounds **1**-**4**. Elucidation of the chemical structures was based on ^{1}H, ^{13}C, COSY experiments for compounds **1**-**2**. Elucidation of the chemical structures was based on ^{1}H and COSY experiments for compounds **3**-**6**. Elemental analyses of C, H, N and S were performed on a Perkin-Elmer 2400 (BioCIS, Châtenay-Malabry, France). Corrected grafting rates (τ_{exp}) are estimated based on the 0.4 % accuracy of the elemental analysis. Centrifugal ultrafiltration was performed using a Rotofix 32A Hettich equipped with a fixed angle rotor 1620A. Adapter for 15- and 50-mL conical tubes were purchased from VWR. Ultrafiltration unit with vertical Omega™ membrane and polypropylene housing (Macrosep® Advance, 10 kDa) were purchased from Pall Laboratory.

4.14. Synthesis of piperazin-1-ium-4-carbodithioate 1

To a solution of piperazine (5.0 g, 58.0 mmol) in MeOH (100 mL) was added CS_2 (3.5 mL, 58.0 mmol, 1.0 equiv). The reaction mixture was stirred at r.t. for 0.5 h. The resulting suspension was then filtered on a frit. The resulting solid was washed with MeOH (2 ×100 mL) and finally dried in vacuo. The desired salt **1** was yielded as a pale-yellow powder (9.26 g, 98 %). ^{1}H NMR (400 MHz, DMSO-d_6) δ 8.49 (2 H, bs), 4.51 (4 H, s), 4.00 (4H, s). ^{13}C NMR (101 MHz, DMSO-d_6) δ 206.7, 55.4, 41.5. Elemental analysis calcd (%) for $C_5H_{10}N_2S_2$ (162.27): C 37.01, H 6.21, N 17.26, S 39.51; found C 37.30, H 6.13, N 16.69, S 39.64.

4.15. Bromopiperazinium dithiocarbamate manganese(I) tetracarbonyl 2

To a solution of **1** (2.2 g, 13.5 mmol) in degassed DCM (30 mL) was added $MnBr(CO)_5$ (3.7 g, 13.5 mmol, 1.0 equiv) at r.t. The reaction mixture was stirred at 45 °C for 4 h. Volatiles were then evaporated under reduced pressure and the resulting solid was finally dried in vacuo. The desired complex **2** was yielded as a yellow powder (5.13 g, 93 %). ^{1}H NMR (400 MHz, DMSO-d_6) δ 8.79z (2 H, bs), 4.02 (4 H, s), 3.23 (4 H, s,). ^{13}C NMR (101 MHz, DMSO-d_6) δ 216.1, 210.7, 206.3, 42.5, 41.7. Elemental analysis calcd (%) for $C_9H_{10}BrN_2O_4S_2$ (409.15): C 26.42, H 2.46, N 6.85, S 15.67; found C 26.25, H 2.36, N 6.37, S 16.03.

4.16. General procedure for the preparation of activated dextrans 3a-d and 4a-d

To a solution of dextran (1.0 g) in anhydrous DMSO (25 mL) was added CDI (τ_{th} + 0.1 equiv). The reaction mixture was stirred at r.t. for 18 h. The mixture was then poured in acetone (150 mL) and the precipitate was filtered on a frit. The resulting solid was successively washed with acetone (150 mL), Et_2O (2 ×150 mL) and finally dried in vacuo.

Activated dextran ***3a***, τ_{th} = 25 % (m = 1.18 g, 100 %). ^{1}H NMR (400 MHz, DMF-d_7) δ 8.45–8.15 (0.25 H, m, >N = C*H*-N =), 7.81–7.57 (0.25 H, m, >N-C*H*=), 7.25–7.05 (0.25 H, m, =N-C*H*=), 5.96–4.41 (4 H, m, $H_{carbamate}$, OH-2, OH-3, OH-4, H-1), 4.31–3.94 (2 H, m, H-3, H-6a), 3.87 (2 H, bs, H-5, H-6b), 3.49–3.20 (1.8 H, m, H-2, H-4). Elemental analysis calcd (%) for $C_{3012}H_{4518}O_{2259}N_{216}$ (79 897): C 45.28, H 5.70, N 3.77; found C 45.41, H 5.52, N 3.12 (τ_{exp} = 20 ± 3 %).

Activated dextran ***3b***, τ_{th} = 50 % (m = 1.23 g, 95 %). ^{1}H NMR (400 MHz, DMF-d_7) δ 8.45–8.15 (0.5 H, m, >N = C*H*-N =), 7.81–7.57 (0.5 H, m, >N-C*H*=), 7.25–7.05 (0.5 H, m, =N-C*H*=), 5.96–4.41 (4 H, m, $H_{carbamate}$, OH-2, OH-3, OH-4, H-1), 4.31–3.94 (2 H, m, H-3, H-6a), 3.87 (2 H, bs, H-5, H-6b), 3.49–3.20 (1.6 H, m, H-2, H-4). Elemental analysis calcd (%) for $C_{3444}H_{4734}O_{2367}N_{432}$ (90 056): C 45.93, H 5.30, N 6.69; found C 45.67, H 5.30, N 6.72 (τ_{exp} = 50 ± 4 %).

Activated dextran ***3c***, τ_{th} = 75 % (m = 1.41 g, 99 %). ^{1}H NMR (400 MHz, DMF-d_7) δ 8.45–8.15 (0.75 H, m, >N = C*H*-N =), 7.81–7.57 (0.75 H, m, >N-C*H*=), 7.25–7.05 (0.75 H, m, =N-C*H*=), 5.96–4.41 (4 H, m, $H_{carbamate}$, OH-2, OH-3, OH-4, H-1), 4.31–3.94 (1.7 H, m, H-3, H-6a), 3.87 (2 H, bs, H-5, H-6b), 3.49–3.20 (1.5 H, m, H-2, H-4). Elemental analysis calcd (%) for $C_{3876}H_{4950}O_{2475}N_{648}$ (100 216): C 46.45, H 4.98, N 9.03; found C 46.52, H 4.97, N 7.97 (τ_{exp} = 63 ± 4 %).

Activated dextran ***3d***, τ_{th} = 100 % (m = 1.53 g, 97 %). ^{1}H NMR (400 MHz, DMF-d_7) δ 8.45–8.15 (1 H, m, >N = C*H*-N =), 7.81–7.57 (1 H, m, >N-C*H*=), 7.25–7.05 (1 H, m, =N-C*H*=), 5.96–4.41 (4 H, m, $H_{carbamate}$, OH-2, OH-3, OH-4, H-1), 4.31–3.94 (1.7 H, m, H-3, H-6a), 3.87 (2 H, bs, H-5, H-6b), 3.49–3.20 (1.3 H, m, H-2, H-4). Elemental analysis calcd (%) for $C_{4308}H_{5166}O_{2583}N_{864}$ (110 376): C 46.87, H 4.72, N 10.93; found C 46.70, H 4.95, N 10.51 (τ_{exp} = 94 ± 5 %).

Activated dextran ***4a***, τ_{th} = 25 % (m = 1.34 g, 100 %). ^{1}H NMR (400 MHz, DMSO-d_6) δ 8.45–8.10 (0.25 H, m, >N = C*H*-N =), 7.78–7.45 (0.25 H, m, >N-C*H*=), 7.25–6.95 (0.25 H, m, =N-C*H*=), 6.45–4.30 (4 H, m, $H_{carbamate}$, OH-2, OH-3, OH-4, H-1), 3.83 (1 H, bs, H-3), 3.75 (1 H, bs, H-6a), 3.72–3.35 (2 H, m, H-5, H-6b), 3.35–2.80 (1.8 H, bs, H-2, H-4). Elemental analysis calcd (%) for $C_{1729}H_{2596}O_{1298}N_{124}$ (45875): C 45.27, H 5.70, N 3.77; found C 45.72, H 5.72, S 4.28 (τ_{exp} = 29 ± 3 %).

Activated dextran ***4b***, τ_{th} = 50 % (m = 1.32 g, 100 %). ^{1}H NMR (400 MHz, DMSO-d_6) δ 8.45–8.10 (0.5 H, m, >N = C*H*-N =), 7.78–7.45 (0.5 H, m, >N-C*H*=), 7.25–6.95 (0.5 H, m, =N-C*H*=), 6.45–4.30 (4 H, m, $H_{carbamate}$, OH-2, OH-3, OH-4, H-1), 3.83 (0.9 H, bs, H-3), 3.77 (1 H, bs, H-6a), 3.72–3.35 (2 H, m, H-5, H-6b), 3.35–2.80 (1.6 H, m, H-2, H-4). Elemental analysis calcd (%) for $C_{1976}H_{2719}O_{1360}N_{247}$ (51684): C 45.92, H 5.30, N 6.69; found C 45.64, H 5.37, S 6.94 (τ_{exp} = 48 ± 1 %).

Activated dextran ***4c***, τ_{th} = 75 % (m = 1.78 g, 100 %). ^{1}H NMR (400 MHz, DMSO-d_6) δ 8.45–8.10 (0.75 H, m, >N = C*H*-N =), 7.78–7.45 (0.75 H, m, >N-C*H*=), 7.25–6.95 (0.75 H, m, =N-C*H*=), 6.45–4.30 (4 H, m, $H_{carbamate}$, OH-2, OH-3, OH-4, H-1), 3.85 (0.9 H, bs, H-3), 3.75 (1 H, bs, H-6a), 3.75–3.25 (2 H, m, H-5, H-6b), 3.25–2.90 (1.4 H, m, H-2, H-4). Elemental analysis calcd (%) for $C_{2223}H_{2843}O_{1421}N_{371}$ (57493): C 46.44, H 4.98, N 9.03; found C 46.67, H 4.92, S 8.89 (τ_{exp} = 73 ± 5 %).

Activated dextran ***4d***, τ_{th} = 100 % (m = 1.75 g, 100 %). ^{1}H NMR (400 MHz, DMSO-d_6) δ 8.45–8.10 (1 H, m, >N = C*H*-N =), 7.78–7.45 (1 H, m, >N-C*H*=), 7.25–6.95 (1 H, m, =N-C*H*=), 6.45–4.30 (4 H, m, $H_{carbamate}$, OH-2, OH-3, OH-4, H-1), 3.85 (0.9 H, bs, H-3), 3.76 (1 H, bs, H-6a), 3.75–3.25 (2 H, m, H-5, H-6b), 3.25–2.90 (1.1 H, m, H-2, H-4). Elemental analysis calcd (%) for $C_{2470}H_{2966}O_{1483}N_{494}$ (63302): C 46.87, H 4.72, N 10.93; found C 47.28, H 4.61, S 10.48 (τ_{exp} = 95 ± 3 %).

4.17. General procedure for the preparation of glyco-CORMs 5a-d and 6a-d

To a suspension of **3** or **4** (1.0–1.5 g) in degassed anhydrous EtOH (50 mL) were successively added **2** (τ_{th} + 0.1 equiv) and NEt_3 (τ_{th} + 0.1 equiv) at r.t. The reaction mixture was stirred at 45 °C for 18 h. Water (10 mL) was then added, and the mixture was stirred from 45 °C to r.t. for 30 min. Volatiles were removed under reduced pressure and Et_2O (50 mL) was added. The suspension was filtrated through a frit and washed twice with Et_2O (50 mL). The powder was then retaken in EtOH (30 mL) and ultrafiltrated by centrifugation (45 min, 60000 rpm). The residual solid was then ultrafiltrated by centrifugation (45 min, 60000 rpm) using EtOH (30 mL) then acetone/water (1:1) mixture. The solid was finally resuspended in Et_2O (50 mL), filtrated on a frit, washed with Et_2O (50 mL) and dried in vacuo.

glyco-CORM ***5a***, τ_{th} = 25 % (m = 990 mg, 73 %). ^{1}H NMR (400 MHz, DMSO-d_6) δ 5.30–4.80 (1.9 H, m, 3-OH, 4-OH), 4.67 (1 H, s, 1-H), 4.53 (0.8 H, s, 2-OH), 4.34 (0.1 H, bs, H-3/$4_{carbamate}$), 4.11 (0.1 H, bs, H-4/$3_{carbamate}$), 3.98 (0.2 H, s, H-$2_{carbamate}$), 3.74 (1 H, s, H-6a), 3.63c (1 H, H-5), 3.60–3.30 (2 H, m, H-3, H-6b), 3.30–2.85 (4 H, m, H-2, H-4, H_{pz}). Elemental analysis calcd (%) for $C_{3660}H_{5058}O_{2691}N_{216}S_{216}Mn_{108}$ (107 956): C 40.69, H 4.73, N 2.79, S 6.40; found C 40.75, H 4.96, N 2.93, S

6.50 (τ_{exp} = 24 ± 5 %).

glyco-CORM ***5b***, τ_{th} = 50 % (m = 1.47 g, 90 %). ^{1}H NMR (400 MHz, DMSO-d_6) δ 5.30–4.80 (1.8 H, m, 3-OH, 4-OH), 4.66 (1 H, s, 1-H), 4.60–4.25 (0.8 H, m, 2-OH, H-3/4$_{carbamate}$), 4.12 (0.1 H, bs, H-4/3$_{carbamate}$), 3.98 (0.3 H, s, H-2$_{carbamate}$), 3.73 (1 H, s, H-6a), 3.62 (1 H, s, H-5), 3.55–3.30 (2 H, m, H-3, H-6b), 3.30–2.85 (5 H, m, H-2, H-4, H$_{pz}$). Elemental analysis calcd (%) for $C_{4740}H_{5814}O_{3231}N_{432}S_{432}Mn_{216}$ (146 202): C 38.91, H 4.01, N 4.14, S 9.47; found C 38.75, H 3.96, N 3.76, S 8.93 (τ_{exp} = 48 ± 7 %).

glyco-CORM ***5c***, τ_{th} = 75 % (m = 1.8 g, 98 %). ^{1}H NMR (400 MHz, DMSO-d_6) δ 5.30–4.80 (1.6 H, m, 3-OH, 4-OH), 4.66 (1 H, s, 1-H), 4.49 (0.6 H, s, 2-OH), 4.42 (0.2 H, bs, H-3/4$_{carbamate}$), 4.12 (0.2 H, bs, H-4/3$_{carbamate}$), 3.99 (0.4 H, s, H-2$_{carbamate}$), 3.73 (1 H, s, H-6a), 3.61 (1 H, H-5), 3.43 (2 H, bs, H-3, H-6b), 3.18 (7 H, bs, H-2, H-4, H$_{pz}$). Elemental analysis calcd (%) for $C_{5820}H_{6570}O_{3771}N_{648}S_{648}Mn_{324}$ (184 448): C 37.86, H 3.59, N 4.92, S 11.27; found C 38.15, H 3.72, N 4.61, S 10.43 (τ_{exp} = 66 ± 4 %).

glyco-CORM ***5d***, τ_{th} = 100 % (m = 2.0 g, 98 %). ^{1}H NMR (400 MHz, DMSO-d_6) δ 5.60–4.80 (1.5 H, m, 3-OH, 4-OH), 4.66 (1 H, s, 1-H), 4.49 (0.5 H, s, 2-OH), 4.40 (0.3 H, bs, H-3/4$_{carbamate}$), 4.12 (0.2 H, bs, H-4/3$_{carbamate}$), 4.00 (0.5 H, s, H-2$_{carbamate}$), 3.73 (1 H, s, H-6a), 3.61 (1 H, H-5), 3.43 (1.7 H, bs, H-3, H-6b), 3.19 (9 H, bs, H-2, H-4, H$_{pz}$). Elemental analysis calcd (%) for $C_{6900}H_{7326}O_{4311}N_{864}S_{864}Mn_{432}$ (222 694): C 37.19, H 3.32, N 5.43, S 12.42; found C 37.09, H 3.48, N 5.33, S 12.08 (τ_{exp} = 94 ± 10 %).

glyco-CORM ***6a***, τ_{th} = 25 % (m = 1.52 g, 98 %). ^{1}H NMR (400 MHz, DMSO-d_6) δ 5.30–4.80 (1.8 H, m, 3-OH, 4-OH), 4.67 (1 H, s, 1-H), 4.53 (0.8 H, s, 2-OH), 4.34 (0.1 H, bs, H-3/4$_{carbamate}$), 4.11 (0.1 H, bs, H-4/3$_{carbamate}$), 3.98 (0.2 H, s, H-2$_{carbamate}$), 3.74 (1 H, s, H-6a), 3.63c (1 H, H-5), 3.60–3.30 (2 H, m, H-3, H-6b), 3.30–2.85 (4 H, m, H-2, H-4, H$_{pz}$). Elemental analysis calcd (%) for $C_{2100}H_{2904}O_{1545}N_{124}S_{124}Mn_{62}$ (61940): C 40.71, H 4.73, N 2.79, S 6.39; found C 40.99, H 4.97, N 1.99, S 5.95 (τ_{exp} = 19 ± 3 %).

glyco-CORM ***6b***, τ_{th} = 50 % (m = 1.96 g, 94 %). ^{1}H NMR (400 MHz, DMSO-d_6) δ 5.30–4.80 (1.7 H, m, 3-OH, 4-OH), 4.66 (1 H, s, 1-H), 4.60–4.25 (0.8 H, m, 2-OH, H-3/4$_{carbamate}$), 4.12 (0.1 H, bs, H-4/3$_{carbamate}$), 3.98 (0.3 H, s, H-2$_{carbamate}$), 3.73 (1 H, s, H-6a), 3.62 (1 H, s, H-5), 3.55–3.30 (2 H, m, H-3, H-6b), 3.30–2.85 (6 H, m, H-2, H-4, H$_{pz}$). Elemental analysis calcd (%) for $C_{2717}H_{3337}O_{1854}N_{247}S_{247}Mn_{124}$ (83814): C 38.94, H 4.01, N 4.13, S 9.45; found C 38.96, H 3.93, N 4.05, S 9.61 (τ_{exp} = 51 ± 3 %).

glyco-CORM ***6c***, τ_{th} = 75 % (m = 2.72 g, 100 %). ^{1}H NMR (400 MHz, DMSO-d_6) δ 5.30–4.80 (1.6 H, m, 3-OH, 4-OH), 4.66 (1 H, s, 1-H), 4.49 (0.6 H, s, 2-OH), 4.42 (0.2 H, bs, H-3/4$_{carbamate}$), 4.12 (0.2 H, bs, H-4/3$_{carbamate}$), 3.99 (0.4 H, s, H-2$_{carbamate}$), 3.73 (1 H, s, H-6a), 3.61 (1 H, H-5), 3.43 (2 H, bs, H-3, H-6b), 3.18 (7 H, bs, H-2, H-4, H$_{pz}$). Elemental analysis calcd (%) for $C_{3335}H_{3769}O_{2162}N_{371}S_{371}Mn_{185}$ (105688): C 37.90, H 3.59, N 4.91, S 11.24; found C 38.02, H 3.62, N 4.97, S 11.23 (τ_{exp} = 75 ± 3 %).

glyco-CORM ***6d***, τ_{th} = 100 % (m = 3.05 g, 96 %). ^{1}H NMR (400 MHz, DMSO-d_6) δ 5.60–4.80 (1.5 H, m, 3-OH, 4-OH), 4.66 (1 H, s, 1-H), 4.49 (0.5 H, s, 2-OH), 4.40 (0.2 H, bs, H-3/4$_{carbamate}$), 4.12 (0.3 H, bs, H-4/3$_{carbamate}$), 4.00 (0.5 H, s, H-2$_{carbamate}$), 3.73 (1 H, s, H-6a), 3.61 (1 H, H-5), 3.43 (1.8 H, bs, H-3, H-6b), 3.19 (9 H, bs, H-2, H-4, H$_{pz}$). Elemental analysis calcd (%) for $C_{3952}H_{4201}O_{2471}N_{494}S_{494}Mn_{247}$ (127561): C 37.21, H 3.32, N 5.42, S 12.42; found C 37.55, H 3.37, N 5.24, S 11.89 (τ_{exp} = 90 ± 4 %).

CRediT authorship contribution statement

R.F. and R.M. conceptualized the idea of glyco-CORMs and supervised the whole study; M.R. supervised the design and synthesis of glyco-CORMs; L.A.B. synthesized all the compounds and carried out their chemical characterization; S.M. conducted most of the biological experiments, data collection and analysis; R.F. and D.E.B. performed selected experiments in cells; R.M. performed blood CO-Hb assays; B.D. formulated the PP solution for *in vivo* studies; Q.M. and H.K. provided hemoCD1 and essential supervision for the measurements of CO in tissues and cells; R.F., S.M., R.M., L.A.B. and M.R. wrote and edited the manuscript; all authors critically read the manuscript.

Declaration of Competing Interest

We declare no conflict of interest

Data Availability

No data was used for the research described in the article.

Acknowledgements

This work was supported by a grant from the Agence National de la Recherche (ANR-19-CE18–0032-01). D.E.B. is supported by a PhD fellowship from the University of Paris-Est Créteil. The authors are grateful for a Visiting Fellowship from IMRB/INSERM to Q.M. The authors thank all the personnel of the animal facility platform at IMRB.

Appendix A. Supporting information

Supplementary data associated with this article can be found in the online version at doi:10.1016/j.phrs.2023.106770.

References

[1] G.S. Drummond, J. Baum, M. Greenberg, D. Lewis, N.G. Abraham, HO-1 overexpression and underexpression: clinical implications, Arch. Biochem. Biophys. 673 (2019), 108073, https://doi.org/10.1016/j.abb.2019.108073.
[2] R. Motterlini, R. Foresti, Heme oxygenase-1 as a target for drug discovery, Antioxid. Redox Signal. 20 (2014) 1810–1826, https://doi.org/10.1089/ars.2013.5658.
[3] R. Foresti, S.K. Bains, T.S. Pitchumony, L.E. de Castro Bras, F. Drago, J.L. Dubois-Rande, C. Bucolo, R. Motterlini, Small molecule activators of the Nrf2-HO-1 antioxidant axis modulate heme metabolism and inflammation in BV2 microglia cells, Pharmacol. Res. 76 (2013) 132–148, https://doi.org/10.1016/j.phrs.2013.07.010.
[4] Y. Tayem, C.J. Green, R. Motterlini, R. Foresti, Isothiocyanate-cysteine conjugates protect renal tissue against cisplatin-induced apoptosis via induction of heme oxygenase-1, Pharmacol. Res. 81 (2014) 1–9, https://doi.org/10.1016/j.phrs.2014.01.001.
[5] R. Hinkel, P. Lange, B. Petersen, E. Gottlieb, J.K. Ng, S. Finger, J. Horstkotte, S. Lee, M. Thormann, M. Knorr, C. El Aouni, P. Boekstegers, B. Reichart, P. Wenzel, H. Niemann, C. Kupatt, Heme oxygenase-1 gene therapy provides cardioprotection via control of post-ischemic inflammation: an experimental study in a pre-clinical pig model, J. Am. Coll. Cardiol. 66 (2015) 154–165, https://doi.org/10.1016/j.jacc.2015.04.064.
[6] K. Sato, J. Balla, L. Otterbein, R.N. Smith, S. Brouard, Y. Lin, E. Csizmadia, J. Sevigny, S.C. Robson, G. Vercellotti, A.M. Choi, F.H. Bach, M.P. Soares, Carbon monoxide generated by heme oxygenase-1 suppresses the rejection of mouse-to-rat cardiac transplants, J. Immunol. 166 (2001) 4185–4194, https://doi.org/10.4049/jimmunol.166.6.4185.
[7] F.A. Wagener, H.D. Volk, D. Willis, N.G. Abraham, M.P. Soares, G.J. Adema, C. G. Figdor, Different faces of the heme-heme oxygenase system in inflammation, Pharmacol. Rev. 55 (2003) 551–571, https://doi.org/10.1124/pr.55.3.5.
[8] F.A.D.T.G. Wagener, J.L. Dasilva, T. Farley, T. Dewitte, A. Kappas, N.G. Abraham, Differential effects of heme oxygenase isoforms on heme mediation of endothelial intracellular adhesion molecule 1 expression, J. Pharmacol. Exp. Ther. 291 (1999) 416–423. ⟨https://pubmed.ncbi.nlm.nih.gov/10490932/⟩.
[9] T. Minamino, H. Christou, C.M. Hsieh, Y. Liu, V. Dhawan, N.G. Abraham, M. A. Perrella, S.A. Mitsialis, S. Kourembanas, Targeted expression of heme oxygenase-1 prevents the pulmonary inflammatory and vascular responses to hypoxia, Proc. Natl. Acad. Sci. U. S. A (2001), https://doi.org/10.1073/pnas.161272598.
[10] B. Wegiel, R. Larsen, D. Gallo, B.Y. Chin, C. Harris, P. Mannam, E. Kaczmarek, P. J. Lee, B.S. Zuckerbraun, R. Flavell, M.P. Soares, L.E. Otterbein, Macrophages sense and kill bacteria through carbon monoxide-dependent inflammasome activation, J. Clin. Invest. 124 (2014) 4926–4940, https://doi.org/10.1172/JCI72853.
[11] J. Cao, S.J. Peterson, K. Sodhi, L. Vanella, I. Barbagallo, L.F. Rodella, M. L. Schwartzman, N.G. Abraham, A. Kappas, Heme oxygenase gene targeting to adipocytes attenuates adiposity and vascular dysfunction in mice fed a high-fat diet, Hypertension 60 (2012) 467–475, https://doi.org/10.1161/HYPERTENSIONAHA.112.193805.
[12] M. Li, D.H. Kim, P.L. Tsenovoy, S.J. Peterson, R. Rezzani, L.F. Rodella, W. S. Aronow, S. Ikehara, N.G. Abraham, Treatment of obese diabetic mice with a

heme oxygenase inducer reduces visceral and subcutaneous adiposity, increases adiponectin levels, and improves insulin sensitivity and glucose tolerance, Diabetes 57 (2008) 1526–1535, https://doi.org/10.2337/db07-1764.
[13] A. Nicolai, M. Li, D.H. Kim, S.J. Peterson, L. Vanella, V. Positano, A. Gastaldelli, R. Rezzani, L.F. Rodella, G. Drummond, C. Kusmic, A. L'Abbate, A. Kappas, N. G. Abraham, Heme oxygenase-1 induction remodels adipose tissue and improves insulin sensitivity in obesity-induced diabetic rats, Hypertension 53 (2009) 508–515, https://doi.org/10.1161/HYPERTENSIONAHA.108.124701.
[14] L.E. Otterbein, B.S. Zuckerbraun, M. Haga, F. Liu, R. Song, A. Usheva, C. Stachulak, N. Bodyak, R.N. Smith, E. Csizmadia, S. Tyagi, Y. Akamatsu, R.J. Flavell, T. R. Billiar, E. Tzeng, F.H. Bach, A.M. Choi, M.P. Soares, Carbon monoxide suppresses arteriosclerotic lesions associated with chronic graft rejection and with balloon injury, Nat. Med. 9 (2003) 183–190, https://doi.org/10.1038/nm817.
[15] R. Motterlini, L.E. Otterbein, The therapeutic potential of carbon monoxide, Nat. Rev. Drug Discov. 9 (2010) 728–743, https://doi.org/10.1038/nrd3228.
[16] L.E. Otterbein, R. Foresti, R. Motterlini, Heme oxygenase-1 and carbon monoxide in the heart: the balancing act between danger signaling and pro-survival, Circ. Res. 118 (2016) 1940–1959, https://doi.org/10.1161/CIRCRESAHA.116.306588.
[17] R. Motterlini, J.E. Clark, R. Foresti, P. Sarathchandra, B.E. Mann, C.J. Green, Carbon monoxide-releasing molecules: characterization of biochemical and vascular activities, Circ. Res. 90 (2002) e17–e24, https://doi.org/10.1161/hh0202.104530.
[18] J.E. Clark, P. Naughton, S. Shurey, C.J. Green, T.R. Johnson, B.E. Mann, R. Foresti, R. Motterlini, Cardioprotective actions by a water-soluble carbon monoxide-releasing molecule, Circ. Res. 93 (2003) e2–e8, https://doi.org/10.1161/01.RES.0000084381.86567.08.
[19] R. Motterlini, P. Sawle, S. Bains, J. Hammad, R. Alberto, R. Foresti, C.J. Green, CORM-A1: a new pharmacologically active carbon monoxide-releasing molecule, FASEB J. 19 (2005) 284–286, https://doi.org/10.1096/fj.04-2169fje.
[20] R. Motterlini, R. Foresti, Biological signaling by carbon monoxide and carbon monoxide-releasing molecules (CO-RMs), Am. J. Physiol. Cell Physiol. 312 (2017) C302–C313, https://doi.org/10.1152/ajpcell.00360.2016.
[21] R. Motterlini, P. Sawle, J. Hammad, B.E. Mann, T.R. Johnson, C.J. Green, R. Foresti, Vasorelaxing effects and inhibition of nitric oxide in macrophages by new iron-containing carbon monoxide-releasing molecules (CO-RMs), Pharmacol. Res. 68 (2013) 108–117, https://doi.org/10.1038/nm817.
[22] S.H. Crook, B.E. Mann, J.A.H.M. Meijer, H. Adams, P. Sawle, D. Scapens, R. Motterlini, [Mn(CO)4{S2CNMe(CH2CO2H)}], a new water-soluble CO-releasing molecule, Dalton Trans. 40 (2011) 4230–4235, https://doi.org/10.1039/C1DT10125K.
[23] L. Braud, M. Pini, L. Muchova, S. Manin, H. Kitagishi, D. Sawaki, G. Czibik, J. Ternacle, G. Derumeaux, R. Foresti, R. Motterlini, Carbon monoxide-induced metabolic switch in adipocytes improves insulin resistance in obese mice, JCI Insight 3 (2018), e123485, https://doi.org/10.1172/jci.insight.123485.
[24] M. Jastroch, A.S. Divakaruni, S. Mookerjee, J.R. Treberg, M.D. Brand, Mitochondrial proton and electron leaks, Essays Biochem. 47 (2010) 53–67, https://doi.org/10.1042/bse0470053.
[25] M.R. Amorim, R. Foresti, D.E. Benrahla, R. Motterlini, L.G.S. Branco, CORM-401, an orally active carbon monoxide-releasing molecule, increases body temperature by activating non-shivering thermogenesis in rats, Temp. (Austin) 9 (2022) 310–317, https://doi.org/10.1080/23328940.2022.2061270.
[26] C.M. Kusminski, P.E. Bickel, P.E. Scherer, Targeting adipose tissue in the treatment of obesity-associated diabetes, Nat. Rev. Drug Discov. 15 (2016) 639–660, https://doi.org/10.1038/nrd.2016.75.
[27] P.A. Hosick, A.A. Alamodi, M.W. Hankins, D.E. Stec, Chronic treatment with a carbon monoxide releasing molecule reverses dietary induced obesity in mice, Adipocyte 5 (2016) 1–10, https://doi.org/10.1080/21623945.2015.1038443.
[28] P.A. Hosick, A.A. Alamodi, M.V. Storm, M.U. Gousset, B.E. Pruett, W. Gray III, J. Stout, D.E. Stec, Chronic carbon monoxide treatment attenuates development of obesity and remodels adipocytes in mice fed a high-fat diet, Int. J. Obes. (Lond.) 38 (2014) 132–139, https://doi.org/10.1038/ijo.2013.61.
[29] H.J. Vreman, R.J. Wong, T. Kadotani, D.K. Stevenson, Determination of carbon monoxide (CO) in rodent tissue: effect of heme administration and environmental CO exposure, Anal. Biochem. 341 (2005) 280–289, https://doi.org/10.1016/j.ab.2005.03.019.
[30] D.K. Stevenson, H.J. Vreman, R.J. Wong, P.A. Dennery, C.H. Contag, Carbon monoxide detection and biological investigations, Trans. Am. Clin. Climatol. Assoc. 111 (2000) 61–75. ⟨https://www.ncbi.nlm.nih.gov/pmc/articles/PMC2194377/⟩.
[31] K. Vanova, J. Suk, T. Petr, D. Cerny, O. Slanar, H.J. Vreman, R.J. Wong, T. Zima, L. Vitek, L. Muchova, Protective effects of inhaled carbon monoxide in endotoxin-induced cholestasis is dependent on its kinetics, Biochimie 97 (2014) 173–180, https://doi.org/10.1080/21623945.2015.1038443.
[32] S. Prabhu, H. Deng, T.L. Cross, S.H. Shahoei, C.J. Konopka, M.N. Gonzalez, C. C. Applegate, M.A. Wallig, L.W. Dobrucki, E.R. Nelson, A.M. Smith, K.S. Swanson, Nanocarriers targeting adipose macrophages increase glucocorticoid anti-inflammatory potency to ameliorate metabolic dysfunction, Biomater. Sci. 9 (2021) 506–518, https://doi.org/10.1039/D0BM01142H.
[33] L. Ma, T.W. Liu, M.A. Wallig, I.T. Dobrucki, L.W. Dobrucki, E.R. Nelson, K. S. Swanson, A.M. Smith, Efficient targeting of adipose tissue macrophages in obesity with polysaccharide nanocarriers, ACS Nano 10 (2016) 6952–6962, https://doi.org/10.1021/acsnano.6b02878.
[34] R.H. Zhang, H.Y. Guo, H. Deng, J. Li, Z.S. Quan, Piperazine skeleton in the structural modification of natural products: a review, J. Enzym. Inhib. Med. Chem. 36 (2021) 1165–1197, https://doi.org/10.1080/14756366.2021.1931861.
[35] M.N. Romanelli, D. Manetti, L. Braconi, S. Dei, A. Gabellini, E. Teodori, The piperazine scaffold for novel drug discovery efforts: the evidence to date, Expert. Opin. Drug Disco 17 (2022) 969–984, https://doi.org/10.1080/17460441.2022.2103535.
[36] E.R. Knight, N.H. Leung, Y.H. Lin, A.R. Cowley, D.J. Watkin, A.L. Thompson, G. Hogarth, J.D. Wilton-Ely, Multimetallic arrays: symmetrical bi-, tri- and tetrametallic complexes based on the group 10 metals and the functionalisation of gold nanoparticles with nickel-phosphine surface units, Dalton Trans. (2009) 3688–3697, https://doi.org/10.1039/B821947H.
[37] C.H. Bamford, I.P. Middleton, K.G. Al-Lamee, Studies of the esterification of dextran: routes to bioactive polymers and graft copolymers, Polymer 27 (1986) 1981–1985, https://doi.org/10.1016/0032-3861(86)90194-1.
[38] A.N. Lukyanov, R.M. Sawant, W.C. Hartner, V.P. Torchilin, PEGylated dextran as long-circulating pharmaceutical carrier, in: J Biomater. Sci. Polym, 15, 2004, pp. 621–630, https://doi.org/10.1163/156856204323046889.
[39] S. Minegishi, A. Yumura, H. Miyoshi, S. Negi, S. Taketani, R. Motterlini, R. Foresti, K. Kano, H. Kitagishi, Detection and removal of endogenous carbon monoxide by selective and cell permeable hemoprotein-model complexes, J. Am. Chem. Soc. 139 (2017) 5984–5991, https://doi.org/10.1021/jacs.7b02229.
[40] F.J. Ruiz-Ojeda, A.I. Ruperez, C. Gomez-Llorente, A. Gil, C.M. Aguilera, Cell models and their application for studying adipogenic differentiation in relation to obesity: a review, Int. J. Mol. Sci. 17 (2016), https://doi.org/10.3390/ijms17071040.
[41] M. Stojak, P. Kaczara, R. Motterlini, S. Chlopicki, Modulation of cellular bioenergetics by CO-releasing molecules and NO-donors inhibits the interaction of cancer cells with human lung microvascular endothelial cells, Pharmacol. Res. 136 (2018) 160–171, https://doi.org/10.1016/j.phrs.2018.09.005.
[42] J.L. Wilson, F. Bouillaud, A.S. Almeida, H.L. Vieira, M.O. Ouidja, J.L. Dubois-Rande, R. Foresti, R. Motterlini, Carbon monoxide reverses the metabolic adaptation of microglia cells to an inflammatory stimulus, Free Rad. Biol. Med. 104 (2017) 311–323, https://doi.org/10.1016/j.freeradbiomed.2017.01.022.
[43] Q. Mao, A.T. Kawaguchi, S. Mizobata, R. Motterlini, R. Foresti, H. Kitagishi, Sensitive quantification of carbon monoxide (CO) *in vivo* reveals a protective role of circulating hemoglobin in CO intoxication, Commun. Biol. 4 (2021) 425, 10.1038/s42003-021-01880-1,https://doi.org/10.1038/s42003-021-01880-1.
[44] R. Foresti, R. Motterlini, Interaction of carbon monoxide with transition metals: evolutionary insights into drug target discovery, Curr. Drug Targets 11 (2010) 1595–1604, https://doi.org/10.2174/1389450111009011595.PM:20704543.
[45] J.I. Odegaard, A. Chawla, The immune system as a sensor of the metabolic state, Immunity 38 (2013) 644–654, https://doi.org/10.1016/j.immuni.2013.04.001.
[46] J.I. Odegaard, R.R. Ricardo-Gonzalez, M.H. Goforth, C.R. Morel, V. Subramanian, L. Mukundan, E.A. Red, D. Vats, F. Brombacher, A.W. Ferrante, A. Chawla, Macrophage-specific PPARgamma controls alternative activation and improves insulin resistance, Nature 447 (2007) 1116–1120, https://doi.org/10.1038/nature05894.
[47] J.M. Monk, D.M. Liddle, A.L. Hutchinson, L.E. Robinson, Studying adipocyte and immune cell cross talk using a co-culture system, Methods Mol. Biol. 2184 (2020) 111–130, https://doi.org/10.1007/978-1-0716-0802-9_9.
[48] R.P. Gullapalli, C.L. Mazzitelli, Polyethylene glycols in oral and parenteral formulations–a critical review, Int. J. Pharm. 496 (2015) 219–239, https://doi.org/10.1016/j.ijpharm.2015.11.015.
[49] T. Loftsson, Cyclodextrins in parenteral formulations, J. Pharm. Sci. 110 (2021) 654–664, https://doi.org/10.1016/j.xphs.2020.10.026.
[50] P. Saokham, C. Muankaew, P. Jansook, T. Loftsson, Solubility of cyclodextrins and drug/cyclodextrin complexes, Molecules 23 (2018), https://doi.org/10.3390/molecules23051161.
[51] R.P. Patel, M.M. Patel, Physicochemical characterization and dissolution study of solid dispersions of Lovastatin with polyethylene glycol 4000 and polyvinylpyrrolidone K30, Pharm. Dev. Technol. 12 (2007) 21–33, https://doi.org/10.1080/10837450601166510.
[52] M. Kurakula, G.S.N.K. Rao, Pharmaceutical assessment of polyvinylpyrrolidone (PVP): as excipient from conventional to controlled delivery systems with a spotlight on COVID-19 inhibition, J. Drug Deliv. Sci. Technol. 60 (2020), 102046, https://doi.org/10.1016/j.jddst.2020.102046.
[53] Z. Zheng, X. Pan, L. Luo, Q. Zhang, X. Huang, Y. Liu, K. Wang, Y. Zhang, Advances in oral absorption of polysaccharides: mechanism, affecting factors, and improvement strategies, Carbohydr. Polym. 282 (2022), 119110, https://doi.org/10.1016/j.carbpol.2022.119110.
[54] Z. Zheng, X. Pan, J. Xu, Z. Wu, Y. Zhang, K. Wang, Advances in tracking of polysaccharides in vivo: labeling strategies, potential factors and applications based on pharmacokinetic characteristics, Int. J. Biol. Macromol. 163 (2020) 1403–1420, https://doi.org/10.1016/j.ijbiomac.2020.07.210.
[55] R. Mehvar, Dextrans for targeted and sustained delivery of therapeutic and imaging agents, J. Control Release 69 (2000) 1–25, https://doi.org/10.1016/S0168-3659(00)00302-3.
[56] Y. Kaneo, T. Uemura, T. Tanaka, S. Kanoh, Polysaccharides as drug carriers: biodisposition of fluorescein-labeled dextrans in mice, Biol. Pharm. Bull. 20 (1997) 181–187, https://doi.org/10.1248/bpb.20.181.
[57] S.Y. Chang, E.J. Weber, K.V. Ness, D.L. Eaton, E.J. Kelly, Liver and kidney on chips: microphysiological models to understand transporter function, Clin. Pharmacol. Ther. 100 (2016) 464–478, https://doi.org/10.1002/cpt.436.
[58] A.W. Basit, J.M. Newton, M.D. Short, W.A. Waddington, P.J. Ell, L.F. Lacey, The effect of polyethylene glycol 400 on gastrointestinal transit: implications for the formulation of poorly-water soluble drugs, Pharm. Res. 18 (2001) 1146–1150, https://doi.org/10.1023/A:1010927026837.
[59] E. Jackson, R. Shoemaker, N. Larian, L. Cassis, Adipose tissue as a site of toxin accumulation, Compr. Physiol. 7 (2017) 1085–1135, https://doi.org/10.1002/cphy.c160038.

[60] J.D. Byrne, D. Gallo, H. Boyce, S.L. Becker, K.M. Kezar, A.T. Cotoia, V.R. Feig, A. Lopes, E. Csizmadia, M.S. Longhi, J.S. Lee, H. Kim, A.J. Wentworth, S. Shankar, G.R. Lee, J. Bi, E. Witt, K. Ishida, A. Hayward, J.L.P. Kuosmanen, J. Jenkins, J. Wainer, A. Aragon, K. Wong, C. Steiger, W.R. Jeck, D.E. Bosch, M.C. Coleman, D. R. Spitz, M. Tift, R. Langer, L.E. Otterbein, G. Traverso, Delivery of therapeutic carbon monoxide by gas-entrapping materials, Sci. Transl. Med. 14 (2022) eabl4135, https://doi.org/10.1126/scitranslmed.abl4135.

[61] Z. El Ali, A. Ollivier, S. Manin, M. Rivard, R. Motterlini, R. Foresti, Therapeutic effects of CO-releaser/Nrf2 activator hybrids (HYCOs) in the treatment of skin wound, psoriasis and multiple sclerosis, Redox Biol. 34 (2020), 101521, https://doi.org/10.1016/j.redox.2020.101521.

[62] K. Kano, H. Kitagishi, C. Dagallier, M. Kodera, T. Matsuo, T. Hayashi, Y. Hisaeda, S. Hirota, Iron porphyrin-cyclodextrin supramolecular complex as a functional model of myoglobin in aqueous solution, Inorg. Chem. 45 (2006) 4448–4460, https://doi.org/10.1021/ic060137b.

[63] S. Fayad-Kobeissi, J. Ratovonantenaina, H. Dabire, J.L. Wilson, A.M. Rodriguez, A. Berdeaux, J.L. Dubois-Rande, B.E. Mann, R. Motterlini, R. Foresti, Vascular and angiogenic activities of CORM-401, an oxidant-sensitive CO-releasing molecule, Biochem. Pharmacol. 102 (2016) 64–77, https://doi.org/10.1016/j.bcp.2015.12.014.

[64] F.L. Rodkey, T.A. Hill, L.L. Pitts, R.F. Robertson, Spectrophotometric measurement of carboxyhemoglobin and methemoglobin in blood, Clin. Chem. 25 (1979) 1388–1393.

[65] R. Motterlini, A. Nikam, S. Manin, A. Ollivier, J.L. Wilson, S. Djouadi, L. Muchova, T. Martens, M. Rivard, R. Foresti, HYCO-3, a dual CO-releaser/Nrf2 activator, reduces tissue inflammation in mice challenged with lipopolysaccharide, Redox Biol. 20 (2019) 334–348, https://doi.org/10.1016/j.redox.2018.10.020.

[66] Y. Kuninobu, Y. Nishina, T. Takeuchi, K. Takai, Manganese-catalyzed insertion of aldehydes into a C-H bond, Angew. Chem. Int. Ed. Engl. 46 (2007) 6518–6520, https://doi.org/10.1002/anie.200702256.